Uncoupling the TFIIH Core and Kinase Modules Leads To Misregulated RNA Polymerase II CTD Serine 5 Phosphorylation

Gabriela Giordano[1], Robin Buratowski[1], Célia Jeronimo[2], Christian Poitras[2]
François Robert[2,3,4], and Stephen Buratowski[1,*]

[1]Department of Biological Chemistry and Molecular Pharmacology,
Harvard Medical School, Boston, MA.

[2]Institut de recherches cliniques de Montréal (IRCM),
Montréal, Québec, Canada

[3]Département de Médecine, Université de Montréal, Montréal, Québec, Canada

[4]Division of Experimental Medicine, Medicine, McGill University, Montréal, Québec, Canada

*Corresponding Author:
steveb@hms.harvard.edu
1-617-432-0696

Abstract

TFIIH is an essential transcription initiation factor for RNA polymerase II (RNApII). This multi-subunit complex comprises two modules that are physically linked in S. cerevisiae by the subunit Tfb3 (MAT1 in metazoans). The Core Module, with two DNA-dependent ATPases and several additional subunits, promotes DNA unwinding. The Kinase Module phosphorylates the C-terminal domain (CTD) of RNApII subunit Rpb1, initiating a cycle of CTD modifications that coordinate exchange of initiation and elongation factors. Why these two disparate activities are bundled into one factor is not obvious, but the connection may provide temporal coordination during early initiation. When Tfb3 is split into two parts to uncouple the TFIIH modules, the resulting cells are viable but grow very slowly. Chromatin immunoprecipitation of the split TFIIH shows that the Core Module, but not the Kinase, is properly recruited to promoters. Instead of the normal promoter-proximal peak, high CTD Serine 5 phosphorylation is seen throughout transcribed regions. Therefore, coupling the TFIIH modules is necessary to localize and limit CTD kinase activity to early stages of transcription. These results are consistent with the idea that the two TFIIH modules began as independent functional entities that later became connected by Tfb3 during early eukaryotic evolution.

Impact Statement: The TFIIH subunit Tfb3/MAT1 can be split into two parts to uncouple the TFIIH kinase and DNA translocase modules, resulting in unfocused CTD phosphorylation.

INTRODUCTION

The three nuclear RNA polymerases in eukaryotes share many features, reflecting their evolution from a single precursor (reviewed in (Vannini & Cramer, 2012)). Their multiple subunits are either homologous or identical, and the initiation factors needed to direct all three polymerases to their appropriate target promoters include both the TATA-Binding Protein (TBP) and a TFIIB-like factor. Extending the parallels, RNA polymerases I and III contain intrinsic subunits that resemble the RNA polymerase II (RNApII) initiation factors TFIIE or TFIIF, which help direct the template DNA into the active site cleft.

In contrast to this overall mechanistic conservation, RNApII initiation factor TFIIH has no obvious counterparts in the other polymerase systems. As the final basal factor to assemble into the Pre-Initiation Complex (PIC), TFIIH performs two functions that are unique to RNApII (Thomas & Chiang, 2006). The first is the use of ATP hydrolysis to accelerate promoter melting, and the second is phosphorylation of a unique C-terminal domain (CTD) on Rpb1, the largest RNApII subunit. These two activities presumably evolved after the divergence of the three RNA polymerases.

The two TFIIH functions map to distinct sub-complexes, sometimes called modules, that are apparent in the TFIIH structure (**Figure 1A**) (He et al., 2016; Robinson et al., 2016; Schilbach et al., 2017). Ssl2 (XPB in metazoans) is the DNA-dependent ATPase that pushes double-stranded DNA towards the RNApII active site, leading to strand separation and placement of the template strand in the polymerase active site (Grünberg et al., 2012). Ssl2/XPB interacts with DNA downstream of RNApII, held in place by six other subunits (Tfb1, Tfb2, Tfb4, Tfb5, Rad3/XPD, and Ssl1) within the “Core” TFIIH subcomplex. TFIIH binding to the PIC is mediated by interactions of the Core with TFIIE and the Rpb4/7 stalk of RNApII (He et al., 2016; Robinson et al., 2016; Schilbach et al., 2017). Interestingly, Rad3 (XPD in metazoans) is a second DNA-dependent ATPase within the core, but with opposite DNA polarity relative to Ssl2/XPB. Surprisingly, Rad3/XPD makes no contact with DNA in PIC structures, and catalytically inactive Rad3 mutants do not affect transcription (Sung et al., 1988; Winkler et al., 2000). It is not obvious why there are so many Core TFIIH subunits with no clear contribution to the promoter melting function other than positioning Ssl2/XPB. One relevant consideration is that TFIIH also functions as a DNA nucleotide excision repair (NER) enzyme. In that process, both TFIIH ATPases unwind DNA to expose a short stretch of the damaged strand for lesion removal (Kim et al., 2023; van Eeuwen, Shim, et al., 2021; Yu et al., 2023). It seems plausible that the TFIIH Core module originally evolved for DNA repair, and only later was co-opted for RNApII transcription.

The second TFIIH sub-complex carries the CTD phosphorylation activity. The Rpb1 CTD is made up of multiple repeats of the sequence YSPTSPS, and its changing phosphorylation patterns help recruit various mRNA processing factors during different stages of the transcription cycle (Buratowski, 2009). The Kin28 (CDK7 in metazoans) kinase and its cyclin partner Ccl1 (Cyclin H) together phosphorylate CTD Serine 5 at the promoter. PIC structures show that the Mediator complex helps guide the CTD to the kinase module (Robinson et al., 2016; Schier & Taatjes, 2021; Schilbach et al., 2017; Schilbach et al., 2023). CTD phosphorylation triggers release of Mediator, as well as subsequent recruitment of mRNA capping enzyme and other factors that function near 5’ ends of mRNAs (reviewed in (Buratowski, 2009)). Like the Core, the Kinase module also has a second function unrelated to transcription. At least in metazoans, CDK7/cyclin H serves as a CDK-activating kinase (CAK), phosphorylating the T-loop

100 of other cyclin-dependent kinases to promote an active conformation (Fisher & Morgan, 1994).
101 This is not a universal function, as *Saccharomyces cerevisiae* and some other species have a
102 separate CAK enzyme (Cismowski et al., 1995; Espinoza et al., 1996; Kaldis et al., 1996).
103 Nonetheless, it seems likely that the CDK7 activity targeting RNApII evolved from a pre-existing
104 CDK that had either CAK activity or some other function.
105 The two TFIIH subcomplexes are linked by the Tfb3 subunit (known as MAT1 in
106 metazoans). Tfb3/MAT1 consists of two globular domains and a linker region. The N-terminal
107 domain contains a zinc-binding RING finger and is part of the Core module, where it helps
108 incorporate TFIIH into the PIC through direct interactions with RNApII and TFIIE (Schier &
109 Taatjes, 2021). The Tfb3 C-terminal domain contacts both the kinase and cyclin subunits, and
110 this interaction promotes an active kinase conformation (Greber et al., 2020; Peissert et al.,
111 2020; van Eeuwen, Li, et al., 2021). In many TFIIH and PIC structures the linker is not visible,
112 presumably due to flexibility. However, when it is seen (Abril-Garrido et al., 2023; Greber et al.,
113 2019), the linker emerges from the N-terminal domain as a long alpha-helix running along the
114 interface between the two ATPase subunits, followed by a turn and a short stretch of helix just
115 N-terminal to a disordered region that connects to the C-terminal region (see schematic in
116 **Figure 1A**). A deletion study in yeast showed that Tfb3 tolerates 30 amino acid deletions
117 throughout the linker, but that the N- and C-terminal domains were essential for viability
118 (Warfield et al., 2016).
119 Given its modular structure, we tested whether other CTD kinases could be fused to
120 Tfb3 to bypass the requirement for Kin28/CDK7. While the results have so far been negative,
121 we unexpectedly found that cells lacking the C-terminal domain of Tfb3 were actually viable,
122 albeit very slow growing. Remarkably, growth is significantly rescued when the two parts of
123 Tfb3 are expressed as separate proteins. In these cells, the TFIIH kinase module is no longer
124 tethered to the Core TFIIH. ChIP experiments show that the Core Module, but not the Kinase, is
125 still promoter localized. Surprisingly, phosphorylation of CTD Serine 5 is now seen at higher
126 than normal levels throughout transcribed regions, indicating that the untethered kinase
127 accesses RNApII throughout the cell cycle. These results are consistent with the idea that the
128 two TFIIH modules began as independent entities that only later became fused into a single
129 complex to provide coordinated regulation of the TFIIH kinase and promoter melting activities.
130
131
132

133 **RESULTS**

134 **Tethering other kinase modules to Tfb3 does not bypass the requirement for Kin28.**
135 Given the apparent modularity of TFIIH, we asked whether tethering other kinases to Tfb3
136 could functionally replace Kin28. Although Kin28 phosphorylates CTD Serine 5 in vivo, other
137 kinases can phosphorylate this residue in vitro. Two other transcription kinase complexes,
138 Bur1/Bur2 (the yeast homologs of CDK9/cyclin T) and Ctk1/Ctk2/Ctk3 (yeast CDK12/Cyclin K),
139 phosphorylate the Rpb1 linker (Chun et al., 2019) and CTD Serine 2 (Cho et al., 2001),
140 respectively. However, both are reported to also have activity on CTD Serine 5, at least in vitro
141 (Corden, 2013; Eick & Geyer, 2013; Glover-Cutter et al., 2009). Accordingly, we constructed
142 Tfb3 fusions **(Figure 1B, Supplemental Table 1)** in which the C-terminal region (C-term) was
143 replaced with either Bur2 (the cyclin partner of Bur1) or Ctk3 (the third subunit within the
144 Ctk1/Ctk2 CDK/cyclin complex). We also created a fusion of the Tfb3 N-terminal domain (N-
145 term) and linker to Mpk1, a single subunit kinase also reported to have activity on CTD Serine 5,
146 as well as Ser2 and Tyr1 (Yurko et al., 2017).

147 The three fusion constructs were introduced into a yeast strain lacking the chromosomal
148 copy of *KIN28*. Expression of the fusion proteins was confirmed by immunoblotting (**Figure 1 –**
149 **figure supplement 1**). None of the fusions supported viability after plasmid shuffling to remove
150 *KIN28* (**Figure 1C**), indicating that tethering the other kinases could not substitute for Kin28
151 function. As a control experiment, the Tfb3 fusions were also tested for complementation of a
152 *TFB3* deletion. Surprisingly, these shuffled strains proved to be viable, albeit so slowly growing
153 that 5-7 days were needed to see colonies **(Figure 1D)**. Complementation of *tfb3Δ* indicates
154 that the fusion proteins were incorporated into TFIIH. This result was unexpected because a
155 *TFB3* allele encoding amino acids 1-275, and therefore lacking the C-term, did not support
156 growth, consistent with earlier reports that the C-terminal domain is essential for Tfb3 function
157 and cell viability (Feaver et al., 2000; Warfield et al., 2016).

158 **The N-terminal domain is the only essential part of Tfb3.** The unexpected
159 complementation of *tfb3Δ* by the Tfb3 fusions raised the question of whether the Tfb3 C-term
160 was truly essential for viability. Earlier studies may not have waited long enough to see growth.
161 Also, the restriction fragment deletion used to create the non-complementing Tfb3(1-275)
162 allele used in **Figure 1D** also removed the 3' untranslated region and polyA site (Feaver et al.,
163 2000), which could further impair function beyond the loss of the C-term. Accordingly, we
164 created a new set of Tfb3 truncations, each lacking either one or two of the three major Tfb3
165 domains **(Figure 2A)**, and used plasmid shuffling to introduce them into a *tfb3Δ* strain. Cells
166 lacking the N-term failed to grow, no matter how long the plates were incubated **(Figure 2B**).
167 In contrast, strains expressing only the N-term, or the N-term and Linker (N-term-Linker)
168 domains, exhibited slow growth. These deletions grew at rates similar to the fusion proteins
169 tested above, arguing that the fused kinase module did not provide an additional function or
170 stability relative to a Tfb3 completely lacking any sequence C-terminal to the Linker region. We
171 therefore conclude that, while important for normal growth, the C-term of Tfb3 (which is part
172 of the Kinase Module) is not essential for viability.

173 **Expression of the TFIIH Core and Kinase Modules as independent complexes.** Recent
174 structural studies show that the C-terminal domain of Tfb3, or its metazoan homolog MAT1,
175 stabilizes an active kinase conformation when bound to Kin28/CDK7 and its partner cyclin
176 (Greber et al., 2020; Peissert et al., 2020; van Eeuwen, Li, et al., 2021). Therefore, the slow

177 growth of strains lacking the Tfb3 C-terminal domain could be due to loss of kinase tethering to
178 the Core Module, to lack of Kin28/CDK7 activation, or both.
179 To test the contribution of the Tfb3 kinase activation function separately from kinase
180 tethering, parts of Tfb3 were expressed as two separate proteins (**Figure 2C**). Strains expressing
181 either the N-term (left panel) or N-term-Linker (right panel) derivatives were transformed with
182 plasmids expressing the indicated C-term constructs. These strains were tested for growth by
183 serial dilution spotting, where the size of single colonies serves as a measure of relative growth
184 rate. Again, strains lacking any C-term domain grew very slowly (Vector, top row). In the N-
185 term strain (left panel), adding wild-type Tfb3 restored growth to normal. Co-expression of the
186 separate N-term and C-term domains noticeably improved growth compared to N-term alone,
187 despite the fact that this strain completely lacks the Linker region. Co-expression of the Linker-
188 C-term construct rescued growth to an even greater extent, although not quite to wild-type
189 rates. Therefore, the Linker does contribute to full function of the Kinase Module.
190 A similar pattern was seen for strains expressing the N-term-Linker construct (**Figure 2C**,
191 right panel). Growth improvement was seen by co-expressing C-term, at least when a high copy
192 plasmid is used to produce more protein. Co-expressing the Linker-C-term construct gave a
193 similar growth improvement at both high and low copy, although no greater than the high copy
194 C-term only construct. Altogether, the co-expression results show that the Tfb3 N-terminal and
195 C-terminal domains can function independently of covalent physical linkage.
196 We considered the possibility that, despite the split Tfb3, the TFIIH Kinase and Core
197 Modules could remain associated through other subunit contacts. To test this possibility, a
198 tandem affinity purification (TAP) tag was used to precipitate full-length, C-term, or Linker-C-
199 term Tfb3 derivatives using IgG beads. While there was some variation in protein expression
200 levels (**Figure 3A**, left panel, lanes 1-4), similar amounts of all three TAP fusions were
201 precipitated with IgG beads (lanes 5-8). The Kinase Module was intact, as subunits Kin28 and
202 Ccl1 interacted with full-length or Tfb3 C-terminal constructs equally well (**Figure 3B**). An in
203 vitro phosphorylation assay using GST-CTD as substrate showed that Kinase Modules from the
204 truncated Tfb3 alleles retained activities similar to or slightly below that of full-length Tfb3
205 (**Figure 3 - figure supplement 1**).
206 In contrast to the Kinase Module, the TFIIH Core Module (monitored by Core subunit
207 Tfb1) no longer associates strongly with the uncoupled Tfb3 C-term derivatives (**Figure 4A**,
208 compare lanes 3 and 4 to full-length Tfb3 in lane 2). The Linker-C-term derivative may retain
209 some weak interaction with the Core, but the Tfb1 levels were just slightly above background
210 binding in the untagged strain (lane 1), and far below that seen with full length Tfb3. We
211 conclude that the split Tfb3 does indeed dissociate the two TFIIH modules.
212 The basal transcription factor TFIIE directly contacts several Core TFIIH subunits,
213 including Tfb3, within the RNApII PIC. Furthermore, TFIIE stimulates TFIIH enzymatic activities,
214 including the kinase (Watanabe et al., 2003). To test how the TFIIE-TFIIH association was
215 affected by the split Tfb3, the TAP-precipitated samples were also immunoblotted for the TFIIE
216 subunits Tfa1 and Tfa2. Whereas full length Tfb3 efficiently pulls down both TFIIE subunits, the
217 separated C-term or Linker-C-term derivatives do not **(Figure 4B)**. This result further indicates
218 that the Kinase Module no longer associates with the TFIIH Core or the RNApII initiation
219 complex upon splitting Tfb3 into two parts.

220 **Uncoupling the TFIIH modules disrupts proper kinase localization.** Given the viability
221 of the split Tfb3 strains, we wondered if the untethered Kinase Module was still delivered to
222 promoters, perhaps via interaction with Mediator. Genome-wide chromatin
223 immunoprecipitation (ChIP-Seq) was used to compare localization of the TFIIH modules in the
224 wild-type and split Tfb3 strains. In cells expressing full-length Tfb3, the Core TFIIH subunit Tfb1
225 showed a strong peak near the transcription start site, reflecting promoter localization in the
226 PIC (**Figure 5A and Figure 5 – figure supplement 1A**, red line**)**. In all three split Tfb3 strains
227 (yellow, blue, and green), the Tfb1 signal was reduced relative to the full-length, but still clearly
228 promoter-localized. Perhaps reflecting reduced PIC formation, a similar reduction was seen for
229 RNApII subunit Rpb1 (**Figure 5D and Figure 5 – figure supplement 1D**). Interestingly, the Tfb1
230 signal was closest to normal in the strain in which the Linker was fused to the N-terminal
231 domain, despite the fact that this strain grew slower than strains with the Linker on the C-
232 terminal domain or missing completely (**Figure 2C**). In contrast to Core TFIIH, the Kin28 ChIP
233 signal, normally localized at promoters in wild-type Tfb3 strains, was completely absent in all
234 the split Tfb3 strains (**Figure 5B** and **Figure 5 – figure supplement 1B**). Therefore, although Core
235 TFIIH is still properly localized, the untethered Kinase Module is no longer efficiently targeted to
236 promoters.
237 **Untethered kinase module leads to aberrant Ser5P patterns.** We expected that loss of
238 Kinase Module recruitment would affect CTD Serine 5 phosphorylation (Ser5P) negatively, with
239 possible indirect effects on Ser2P and overall elongation processivity. This prediction was first
240 tested using immunoblotting of whole cell extracts. Cells lacking any Tfb3 C-term were strongly
241 reduced for both Ser5P and Ser2P (**Figure 5 – figure supplement 2**, lanes 2 and 3). Similar to the
242 growth phenotypes, adding back the C-term as a separate protein greatly improved CTD
243 phosphorylation levels at both sites, albeit not to full wild-type levels (lanes 4 and 5).
244 ChIP-seq was used to determine the location of Ser5P, normalizing to spiked-in *S. pombe*
245 chromatin. Surprisingly, the restored Ser5P was abnormally distributed in split Tfb3 cells. Total
246 RNApII crosslinking (**Figure 5D and Figure 5 – figure supplements 1D and 3A, B**) was reduced in
247 the mutants, but the levels remained consistent across the gene. This pattern argues against an
248 elongation processivity defect in the split Tfb3 strains, and contrasts with the 5' to 3' drop seen
249 upon complete depletion of Kin28 (Wong et al., 2014) or Bur2, the cyclin for the elongation
250 kinase Bur1/Cdk9 (Keogh et al., 2003). Ser5P normally has a strong peak at promoters, and
251 lower but significant levels throughout transcribed regions, as can be seen in both individual
252 gene traces (**Figure 5 – figure supplement 3A, B**, promoters in green boxes) and metagene
253 analysis (**Figure 5C** and **Figure 5 – figure supplement 5C**, red curves). In the split Tfb3 strains,
254 the Ser5P promoter peak was missing, but levels of this modification remained high throughout
255 the downstream transcribed region. Normalization of Ser5P to total RNApII indicated that
256 downstream Ser5P was actually elevated in the mutants relative to wild-type (**Figure 5E**).
257 Quantitation of RNApII-normalized Ser5P at individual genes (**Figure 5 -figure**
258 **supplement 1E, F**) showed that this redistribution of Ser5P occurred at virtually all genes. The
259 Ser5P signals at promoters are reduced by up to 50%, particularly at strongly transcribed genes
260 (i.e. those with highest RNApII occupancy), while the distribution for the mutant/WT ratio is
261 centered around one for the weakest genes (**Figure 5 – figure supplement 1E**, left panels). In
262 contrast, the normalized Ser5P signal in open reading frames (right panels) are nearly all
263 increased by two-fold or more in the mutants. Despite the changes in CTD phosphorylation, the

264 steady RNApII levels across genes in the mutants (**Figure 5D**) suggest no defect in elongation
265 processivity. Using the total Rpb1 signals as a measure of transcription levels, it can be seen
266 that transcription is clearly down overall in the split Tfb3 strains (**Figure 5 - figure supplement**
267 **1F**). Isolated analyses of genes that were longer than average, expressed at different levels, or
268 that were more or less dependent on TFIID for initiation showed no differences from the total
269 (**Figure 5 – figure supplement 4A-C**). Notably, seven genes showed an opposite effect from the
270 general drop in transcription, with reproducibly increased Rpb1 signals in the mutants. All but
271 one of these are known heat shock response genes (**Figure 5 – figure supplement 1G**),
272 suggesting these slow growing cells are under stress.
273 ChIP-seq was also performed for Ser2P. While the overall signals were too low to get
274 good quality data for metagene analysis, individual gene traces at strongly transcribed genes
275 suggested that the pattern of Ser2P was relatively normal (**Figure 5 – figure supplement 3B**). In
276 both WT and split Tfb3 strains, Ser2P was lowest near the promoter and gradually increased
277 further downstream.
278 The surprising increase of Ser5P downstream of the promoter suggests that the Tfb3
279 linkage not only delivers the Kinase Module to the promoter, but may also inhibit its activity
280 outside of the PIC. Transcription-associated phosphatases normally cause Ser5P to drop soon
281 after RNApII enters the body of the gene (reviewed in (Buratowski, 2009; Corden, 2013; Eick &
282 Geyer, 2013)), so the higher downstream Ser5P signal suggests untethered kinase module may
283 be able to continually access the CTD during elongation. This could be due to inhibition of TFIIH
284 Core-associated Kinase outside of the PIC, or suggest that the majority of TFIIH is sequestered
285 at promoters and therefore unavailable at later stages of transcription.
286 **Split Tfb3 does not cause an NER defect.** The TFIIH Core Module also functions as a key
287 component of the NER machinery, and Tfb3 has been shown to be important for this function
288 (Feaver et al., 2000). While many mutations in Core subunits therefore cause sensitivity to
289 ultraviolet (UV) light, this is not the case for Kinase Module mutants. Recent structures
290 (reviewed in (van Sluis et al., 2025; Yu et al., 2023)) suggest that the Kinase Module would block
291 interactions between the Core Module and other NER factors. Therefore, TFIIH either enters
292 into the NER complex as free Core Module, or the Kinase Module may dissociate soon after. We
293 tested the response to UV light in strains where the split Tfb3 dissociates the Core and Kinase
294 Modules (**Figure 6**). Two wild-type Tfb3 strains acted as controls for normal UV response,
295 including one strain lacking the Tfb6 protein that competes with the Core for Ssl2 binding
296 (Murakami et al., 2012), as this background was used for many experiments here (see
297 **Supplemental Table S2**). None of the split Tfb3 configurations caused UV sensitivity, indicating
298 that the separated N-term of Tfb3 suffices for the Core NER function. In fact, we noticed that
299 strains with free N-term domain, where the linker is either absent or connected to the C-
300 terminal domain, may even have slight resistance to UV light, consistent with a model in which
301 the Kinase Module inhibits the TFIIH NER function. Any NER role for the kinase module must be
302 functional even in the split Tfb3.
303

304 **DISCUSSION**

305 We show here that the TFIIH Core and Kinase Modules can be uncoupled in vivo, leading
306 to misregulated CTD phosphorylation (**Figure 2**). Although it was previously reported that both
307 the N-term and C-term of Tfb3 are essential for viability in *S. cerevisiae* (Feaver et al., 2000;
308 Warfield et al., 2016), we found that cells lacking the C-terminal domain are viable but
309 extremely slow growing. Consistent with this finding, accurate transcription initiation can be
310 reconstituted in vitro using a Tfb3 truncation consisting of only N-term residues 1-148 (Yang et
311 al., 2022). Furthermore, Mouse Embryonic Fibroblasts and cardiomyocytes with a homozygous
312 deletion of *MAT1* were shown to be viable but abnormal (Helenius et al., 2011; Sano et al.,
313 2007). In these cells, Core TFIIH remains intact, but levels of the Kinase Module proteins CDK7
314 and Cyclin H are severely reduced. *MAT1* deletion leads to major defects in CTD
315 phosphorylation and transcription, but the effects are partially compensated by reduced mRNA
316 degradation rates. Therefore, our results splitting the Core and Kinase Modules in yeast are
317 likely also relevant to mammalian TFIIH.

318 While fusion of other kinase modules to the Tfb3 linker did not substitute for the C-term
319 (**Figure 1**), we found that adding back the Tfb3 C-terminal domain as a separate protein
320 dramatically improved growth (**Figure 2**). As discussed below, this rescue apparently results
321 from the restored CTD kinase activity of the untethered Tfb3 C-term/Kin28/Ccl1 complex
322 (**Figure 3, Figure 3 – figure supplement 1, Figure 5 – figure supplement 2**). ChIP-Seq showed
323 that Kin28 kinase was no longer preferentially recruited to promoters in the split Tfb3 strains,
324 even though Core TFIIH still showed proper localization (**Figure 5 and Figure 5 – figure**
325 **supplement 1**). Having uncoupled the Kinase Module from TFIIH, we expected CTD Ser5P to be
326 severely reduced in the split Tfb3 strains. Indeed, Ser5P peaks at promoters were largely gone,
327 but instead the modification was found throughout the downstream transcribed region at
328 levels higher than normal **Figure 5, Figure 5 – figure supplements 1 and 3**).

329 Several models could explain the abnormal Ser5P pattern seen in strains with split Tfb3.
330 One possibility is that a kinase other than Kin28 somehow substitutes for Ser5 phosphorylation,
331 but without promoter-proximal targeting. However, several observations argue against a
332 compensating kinase. First, any such kinase does not relieve the requirement for *KIN28* in
333 supporting viability (**Figure 1C**). Second, reintroduction of the separated Tfb3 C-term markedly
334 rescues CTD phosphorylation (**Figure 5 – figure supplement 2**), and it is unclear how a kinase
335 other than Kin28 would respond in this manner. Finally, repeated attempts to introduce a
336 chemically inhibitable Kin28 allele (Chun et al., 2019; Joo et al., 2019) into the split Tfb3
337 background were unsuccessful, and this apparent synthetic lethality further suggests that Kin28
338 supplies the essential Ser5 phosphorylation when the TFIIH modules are separated. We
339 therefore consider the compensating kinase model unlikely.

340 A second possibility is that, under normal conditions, the majority of Kinase Module is
341 tethered to the Core at promoters and thereby sequestered from phosphorylating downstream
342 RNApII. Breaking the Tfb3 tether could free the Kinase Module to access the CTD throughout
343 transcription. Arguing against this model, single molecule tracking in vivo reveals substantial
344 fractions of freely diffusing Kin28 and core TFIIH (Nguyen et al., 2021). Furthermore, a
345 significant amount of free CDK7/Cyclin H/MAT1 trimer exists in metazoans, providing CAK
346 activity, and free trimer complex is also detected in yeast extracts (Keogh et al., 2002). On the
347 other hand, the mammalian trimer complex appears to be largely cytoplasmic (Rimel et al.,

348 2020). Therefore, a tethering model might be feasible if Kinase Module containing the Tfb3 C-
349 term is more abundant in the nucleus than that with full-length Tfb3.
350 Both chromatin immunoprecipitation (Bataille et al., 2012; Komarnitsky et al., 2000;
351 Mayer et al., 2010; Tietjen et al., 2010) and mass spectrometry (Suh et al., 2016) show that a
352 low level of Ser5P persists during late elongation. The downstream Ser5P has been presumed to
353 be residual phosphatase-resistant Ser5P acquired at the promoter. However, it is interesting to
354 consider the possibility that free Kinase Module in the nucleus might prevent complete Ser5P
355 dephosphorylation by providing additional de novo phosphorylation during late transcription.
356 This antagonism would be similar to CTD Ser2, where both Ctk1 kinase and Fcp1 phosphatase
357 appear to function throughout elongation (Cho et al., 2001).
358 A third possible explanation for the increase in downstream Ser5P is that untethered
359 Kinase Module can access the CTD during elongation in a way that intact TFIIH cannot. In
360 addition to delivering the kinase to the initiation complex, the connected Core Module might
361 limit CTD phosphorylation when TFIIH is outside of the PIC. Supporting this idea, we previously
362 showed that CTD kinase activity of free trimer Kinase Module was less sensitive than TFIIH
363 complex to mutations in the activating T-loop (Keogh et al., 2002). Also, Rimel et al. showed
364 that the mammalian TFIIH core module significantly inhibits the activity of the mammalian
365 CDK7/CycH/MAT1 complex, at least on substrates other than the CTD (Rimel et al., 2020). These
366 results suggest the Core module has some restrictive effect on CTD kinase activity.
367 In addition to the Core modulating TFIIH Kinase activity, there appears to be
368 communication in the other direction as well. Available TFIIH structures and our data suggest
369 that the Tfb3 linker does more than simply tether the N- and C-terminal domains, as cells
370 expressing a Linker-C-term fusion grew better than cells completely lacking the linker.
371 Comparison of the structures for free TFIIH complex, TFIIH incorporated into the PIC, and TFIIH
372 as part of the NER machinery (reviewed in (van Sluis et al., 2025; Yu et al., 2023)) suggest a
373 second possible linker function. The Core Module has a horseshoe shape, with the TFIIH
374 ATPases, Ssl2/XPB and Rad3/XPD, at the two ends (see **Figure 7** schematic). The spacing
375 between the ATPases changes substantially depending on context. In free TFIIH, the long alpha-
376 helix in the Tfb3/MAT1 Linker spans from Tfb3 N-term, which contacts Rad3/XPD, to the other
377 side of the horseshoe, where it directly contacts Ssl2/XPB (**Figure 7A**). Here, the central Linker
378 domain may lock together the two TFIIH ATPases in a "closed" conformation. In the PIC, the
379 Tfb3/MAT1 alpha-helix is disconnected from Ssl2/XPB, producing an "open" conformation with
380 the Ssl2/XPB rotated outward, its active site bound to the double-stranded DNA downstream of
381 RNApII (**Figure 7B**). TFIIH within the NER complex lacks the Kinase Module, and in this case the
382 NER factors bring Rad3/XPD and Ssl2/XPB even closer together to facilitate the interaction of
383 the damaged DNA with both ATPase active sites (van Sluis et al., 2025; Yu et al., 2023).
384 A report describing two PIC structures assembled in the context of a +1 nucleosome
385 (Abril-Garrido et al., 2023) shows that when the nucleosome blocks Ssl2/XPB from downstream
386 DNA, TFIIH is in the closed conformation, with the Tfb3/MAT1 Linker contacting both ATPases.
387 Positioning the nucleosome further downstream allows the open TFIIH conformation, resulting
388 in loss of the contact between the Tfb3/MAT1 Linker and Ssl2/XPB binding DNA. Notably, much
389 of the Tfb3 long alpha-helix becomes disordered when disconnected from Ssl2/XPB. Although
390 these two PIC structures lack Mediator, and it hasn't been shown that the closed TFIIH PIC is a
391 necessary precursor to the open TFIIH, it seems quite plausible that TFIIH enters the PIC in the

392 closed conformation, transitioning to the open conformation upon DNA binding in order to
393 proceed with DNA translocation and promoter melting.
394 Based on our findings, we speculate that the Tfb3 Linker provides a mechanism for
395 temporal coupling of TFIIH kinase and promoter melting functions (**Figure 7B**). PICs with closed
396 TFIIH are predicted to be inhibited for ATP hydrolysis by Ssl2/XPB (Abril-Garrido et al., 2023),
397 and as described above, may also be partially inhibited for kinase activity (Keogh et al., 2002;
398 Rimel et al., 2020). Movement of the Kinase Module during PIC assembly may reposition the
399 Tfb3 Linker to release the inhibitory contact with Ssl2/XPB, freeing the translocase for promoter
400 melting. This movement might be triggered by capture of the Kinase Module by Mediator, or
401 possibly by initiation of CTD phosphorylation. Alternatively, DNA binding and translocation by
402 Ssl2/XPB in the PIC might release the Linker contact to promote Kinase Module activity. CTD
403 phosphorylation triggers release of Mediator (Sogaard & Svejstrup, 2007), and in vivo
404 experiments with TFIIH kinase inhibition suggest this transition occurs very rapidly after PIC
405 formation (Jeronimo & Robert, 2014; Wong et al., 2014). Notably, release of the Tfb3 Linker
406 contact also results in the long alpha-helix becoming disordered (Abril-Garrido et al., 2023),
407 which could allow the kinase access to a far larger radius of area. This flexibility could help the
408 kinase reach both proximal and distal repeats within the CTD, which can theoretically extend
409 quite far from the RNApII body. Supporting the idea that the Kinase Module is mobile, PICs
410 formed in vitro without Mediator show the Kinase Module close to the Rpb4/Rpb7 stalk of
411 RNApII (Abril-Garrido et al., 2023; Chen et al., 2021), far from its position seen when interacting
412 with Mediator.
413 One species-specific feature of yeast PICs is that they can access transcription start sites
414 (TSSs) far further downstream than metazoan PICs. Enzymatic studies show that for yeast TFIIH,
415 but not its mammalian homolog, the Kinase Module greatly stimulates the processivity of the
416 Ssl2 translocase activity necessary for downstream TSS scanning (Tomko et al., 2021), likely via
417 the interaction of Tfb3 with RNApII. Yeast transcription reconstituted in vitro with TFIIH lacking
418 Tfb3 and the Kinase Module causes a dramatic upstream shift in transcription start sites, with
419 the TATA-TSS spacing now resembling that of metazoans (Murakami et al., 2015). This effect
420 can be reversed by adding back only the Tfb3 N-term (Yang et al., 2022), arguing against a
421 model where the contact between Tfb3 linker and Ssl2 is necessary for downstream TSS usage.
422 Nevertheless, there is clearly some communication between the Kinase and Core Modules, and
423 Tfb3 is likely to be a key link.
424 *Evolutionary considerations.* We speculate that cells with a complete deletion of the
425 Tfb3 Linker may resemble an evolutionarily ancient state where TFIIH Kinase and Core existed
426 as completely distinct enzymes. Initially, the primary role of TFIIH Core was probably NER, and
427 the Kinase Module precursor likely functioned to phosphorylate CDKs or other substrates. Each
428 module would have then been independently co-opted for RNApII transcription. Supporting this
429 hypothesis, TFIIH from the early diverged eukaryote *Trypanosome brucei* appears to consist of
430 only the Core Module, as no Tfb3 or other Kinase Module homologs are detected in the purified
431 enzyme complex or by sequence similarity search (Lee et al., 2010; Lee et al., 2009). The CTD of
432 *T. brucei* Rpb1 is quite diverged, without the typical repeat sequence found in most eukaryotes
433 (Badjatia et al., 2013; Das & Bellofatto, 2009). Similarly, protein sequence searches find no
434 unambiguous TFIIH kinase/cyclin homologs among the cyclin-dependent kinases in *T. brucei* or
435 *Giardia lamblia* (Guo & Stiller, 2004, 2005). In *Plasmodium falciparum*, which also lacks a

436 consensus CTD, a putative Tfb3/MAT1 homolog has been described (Callebaut et al., 2005;
437 Chen et al., 2006). However, this protein has not yet been shown to associate with TFIIH and
438 there is still some uncertainty whether an associated kinase is homologous to Kin28/CDK7 or
439 another CDK.
440 Overall, it appears likely the Tfb3 Linker evolved very early in the eukaryotic lineage,
441 perhaps to coordinate the timing of CTD phosphorylation and promoter melting. In the split
442 Tfb3 strains, fusion of Linker to the C-term domain may improve growth relative to the
443 complete Linker deletion (**Figure 2C**) by partially restoring kinase-translocase coupling. Our
444 ChIP-Seq results suggest an ancestral, free CTD kinase may have acted throughout elongation.
445 Tethering the kinase to TFIIH would have targeted high levels of CTD phosphorylation during
446 early transcription, establishing the first step of the sequential CTD cycle as we know it today,
447 where distinct phosphorylation patterns mark the progression from early through late
448 transcription.
449
450

451 **METHODS**
452
453 **Plasmid construction and Yeast Strains**. Plasmids used in this study, and their
454 construction, are listed in **Supplemental Table S1**. Yeast strains used in this study are listed in
455 **Supplemental Table S2**.
456 **Antibodies and Immunoblotting.** The following primary antisera were used: anti-Ccl1
457 (Keogh et al., 2002), anti-Kin28 (Covance, PRB-250C-500), anti-Tfb1 (Matsui et al., 1995), anti-
458 Tfa1 and anti-Tfa2 (Kuldell & Buratowski, 1997), anti-Ser2P (3E10), anti-Ser5P (3E8) (gift from
459 Dirk Eick (Chapman et al., 2007)), anti-CTD (8WG16) , anti-Rpb3 monoclonal 1Y26 (BioLegend).
460 For immunoblotting, primary antibodies were used at a 1:1000 dilution. Secondary antibodies
461 coupled to horse radish peroxidase (goat anti-rabbit, goat anti-rat, and goat anti-mouse) were
462 purchased from Sigma and used at the recommended dilution.
463 Anti-Tfb3 antibodies (Keogh et al., 2002) were affinity purified from sera to reduce
464 cross-reacting signals. Briefly, recombinant Tfb3 protein was expressed from plasmid
465 pSBEThis7-Tfb3 in *E. coli* BL21(DE3). Cells were grown at 37°C to an OD_{600} of 0.4-0.6 in 4 L of
466 selective media. Expression was induced with 0.2 mM IPTG and cultures were incubated
467 shaking at 30°C for 4 hrs. Cells were pelleted and resuspended in 100 mL lysis buffer (1X PBS,
468 1% SDS, pH 7.4). After sonication, cell debris was pelleted at 23,970 g for 20 min. The
469 supernatant was filtered and then incubated with nutation at 4°C for 1 hr with Ni-NTA agarose
470 (Gold Biotechnology #H-350-100) that was pre-equilibrated with lysis buffer. Lysate and beads
471 were drained through a column and washed extensively with wash buffer (1X Phosphate
472 Buffered Saline (PBS), 0.1% Sarkosyl, 10 mM imidazole, pH 7.4). Bound protein was serially
473 eluted with elution buffer (1X PBS, 0.1% Sarkosyl, pH 7.4) supplemented with increasing
474 imidazole concentrations (1 mL each): 50 mM, 100 mM, 150 mM (2X), 200 mM, 300 mM.
475 Fractions with the highest Tfb3 yield were pooled. Roughly 2 mg of purified Tfb3 was
476 covalently linked to 1 ml AminoLink® Plus Coupling Resin (Thermo Scientific #PI20505) following
477 the manufacturer's protocol for crosslinking at pH 10 with cyanoborohydride solution. Specific
478 anti-Tfb3 antibodies were affinity purified from crude antiserum as described (Harlow & Lane,
479 1988). Tfb3-coupled beads were serially washed with 10 bed volumes each of 10 mM Tris pH
480 7.5, 100 mM glycine pH 2.5, 10 mM Tris pH 8.8, and then 100 mM triethylamine pH 11.5.
481 Finally, beads were poured into a small column and washed with 10 mM Tris pH 7.5 until pH
482 reached 7.5. Antiserum was diluted 1:10 with 10 mM Tris pH 7.5 and passed through the
483 column three times. The column was then washed with 20 bed volumes each of 10 mM Tris pH
484 7.5 and 500 mM NaCl, and then 10 mM Tris pH 7.5. Bound antibodies were serially eluted with
485 small volumes of high (100 mM triethylamine pH 11.5) and low (100 mM glycine pH 2.5) pH,
486 followed by rapid neutralization. Peak fractions were pooled and concentrated using Amicon
487 Ultra 0.5 10K Concentrator, with PBS as the replacement buffer.
488 **Yeast whole cell extracts.** Two types of extracts were used for gel electrophoresis and
489 immunoblotting, with similar results. The first is an alkaline lysis method. 1.5 mL of late log
490 phase liquid culture was pelleted at 4,600 g for 90 sec at room temperature. Media was
491 removed, and the pellet was resuspended in 0.1 M NaOH and incubated at room temperature
492 for 5 min. Cells were pelleted at 9,300 g for 90 sec at room temperature, supernatant was
493 removed, and pellet was resuspended in 60 µL lysis buffer (0.06 M Tris-HCl pH 6.8, 5% glycerol,
494 2% SDS, 4% β-mercaptoethanol, 0.0025% bromophenol blue) (Kushnirov, 2000). Samples were

495 heated at 95°C for 5 min, pelleted at 9,300 g for 1:30 min at room temperature, and
496 supernatant was collected to run on an SDS-PAGE gel.
497 For some gels, a non-denaturing whole cell extract was used. First, 1.0-1.5 mL of liquid
498 culture was pelleted (all centrifugations were at 2,300 g) at 4°C for 2 min and washed with 1 mL
499 cold distilled water. Pellets were resuspended in 100 μL cold lysis buffer (50 mM HEPES pH 7.6,
500 1 mM EDTA, 300 mM NaCl, 20% glycerol, 1 mM DTT, 1 μg/mL leupeptin, 1 μg/mL aprotinin,
501 1 μg/mL pepstatin A, and 1 μg/mL antipain). The resuspension was mixed with 100 μL 425-600
502 μm glass beads (Sigma, #G8772-1KG) and vortexed at 4°C for 10 min. Extract was centrifuged
503 for 10 min at 4°C and supernatant collected. Total protein concentration of extracts was
504 measured using NanoDrop 2000 Spectrophotometer (ThermoScientific)**.**
505 **TAP purification and co-precipitation assay**. TAP-tagged Tfb3 derivatives were used for
506 assaying Kinase Module association and in vitro kinase assays. Yeast strains were grown in 200
507 mL of selective media at 30°C to an OD_{600} of ~2. Cells were collected by centrifugation, flash
508 frozen in liquid nitrogen, and lysed using a SPEX SamplePrep Freezer Mill 6875D with small
509 chambers. Pulverized cells were resuspended by rotation at 4°C in 1 mL of lysis buffer (20 mM
510 HEPES pH 7.6, 10% glycerol, 200 mM KoAc, 1 mM EDTA, 1 mM DTT, 1 mM NaF, 1 mM Na3VO4,
511 1 μg/mL leupeptin, 1 μg/mL aprotinin, 1 μg/mL pepstatin A, 1 μg/mL antipain, 1 mM PMSF)
512 until homogeneous. Cell debris was pelleted in a benchtop microfuge at 4,500 g for 25 min, and
513 supernatant was collected and further cleared in a microfuge at maximum speed for 10 min. All
514 centrifugations were done at 4°C. The clear layer of lysate was transferred to a new tube, 10 μL
515 of IgG Sepharose (GE Healthcare, #17096901) pre-equilibrated with lysis buffer was added, and
516 the suspension was rotated at 4°C for 1 hr. After binding, IgG beads were gently pelleted,
517 supernatant was removed, and beads were washed 3 times with lysis buffer.
518 For analysis of bound proteins, 50 μL of 2X SDS-PAGE sample buffer (0.1% bromophenol
519 blue, 0.2 M DTT, 20% glycerol, 4% SDS, 0.1 M Tris-Cl pH 6.8) were added to the beads and the
520 sample was heated at 100°C for 5 min. The beads were then pelleted by centrifugation,
521 supernatant was collected, and samples were analyzed by immunoblotting. Input, flowthrough,
522 and final samples from the co-immunoprecipitation protocol were run on 10% polyacrylamide
523 SDS-PAGE gels. Proteins were transferred to polyvinylidene difluoride (PVDF) membranes.
524 Membranes were blocked with 5% powdered milk in Tris Buffered Saline with 0.1% Tween and
525 then probed with the appropriate primary antibody. Blocking and antibody incubations were
526 done for either 1 hr at room temperature or overnight at 4°C. Following several washes, the
527 blots were incubated with secondary antibody at a 1:10,000 dilution for 1 hr. Reacting bands
528 were detected by chemiluminescent detection using the Thermo SuperSignal Plus Pico kit
529 according to the manufacturer's instructions.
530 **In vitro CTD phosphorylation assay.** IgG beads were used to immobilize the Tfb3-TAP
531 derivatives as described above. After normalizing for the amount of Kin28, beads were
532 incubated with 100 ng GST-CTD in 1x kinase reaction buffer (20 mM HEPES pH 7.6, 7.5 mM
533 MgOAc, 2% Glycerol, 100 mM KOAc, 2 mM DTT, and 25 μM ATP). Samples were taken at 15, 30,
534 and 60 min, and phosphorylation was assayed by immunoblotting with anti-Ser5P (3E8)
535 antibody.
536 **ChIP-seq.** ChIP experiments were performed from two independent biological replicates
537 as previously described (Jeronimo et al., 2021). Yeast cultures were grown in 50 mL of selective
538 medium at 30°C to an OD_{600} of 0.7-0.9 before crosslinking with 1% formaldehyde (Fisher

539 Scientific, BP531-500) at room temperature for 30 min and quenched with 125 mM glycine.
540 Crosslinked cells were collected by centrifugation and washed twice with 1X TBS (20 mM Tris-
541 HCl pH 7.5, 150 mM NaCl). Cell pellets were then resuspended in 700 µL Lysis buffer (50 mM
542 HEPES-KOH pH 7.5, 140 mM NaCl, 1 mM EDTA, 1% Triton X-100, 0.1% Na-deoxycholate and
543 protease inhibitor cocktail (1 mM PMSF, 1 mM benzamidine, 10 µg/mL aprotinin, 1 µg/mL
544 leupeptin, 1 µg/mL pepstatin A)). About the same number of OD_{600} units was used for all
545 samples. A fixed amount of crosslinked *Schizosaccharomyces pombe* cells (a gift from Jason
546 Tanny), at 10% the amount of *S. cerevisiae* cells, was added for normalization as previously
547 described (Jeronimo et al., 2019). Cells were lysed by bead beating and the lysate was sonicated
548 with a Model 100 Sonic dismembrator equipped with a microprobe (Fisher Scientific), 4 x 20 sec
549 at output 7 Watts, with a 1 min break between sonication cycles. Soluble fragmented
550 chromatin was recovered by centrifugation. 600 µL of the chromatin sample was taken per
551 immunoprecipitation (IP) and 6 µL (1%) was saved as an Input sample. The following amounts
552 of antibody per IP were used: anti-RNApII Rpb1 8WG16 (2 µg), anti-Ser5P 3E8 (5 µL), anti-Tfb1
553 (4 µL) and anti-Kin28 (4 µL). All antibodies have been validated for ChIP. Anti-Ser5P 3E8, anti-
554 Tfb1, and anti-Kin28 antibodies were coupled to Dynabeads coated with Protein G (Thermo
555 Fisher Scientific, 10004D) and anti-RNApII Rpb1 8WG16 antibody was coupled to Dynabeads
556 coated with Pan Mouse IgG antibodies (Thermo Fisher Scientific, 11042). 50 µL of the
557 appropriate Dynabeads pre-coupled with the indicated antibody were added to the chromatin
558 sample and incubated overnight at 4°C. Beads were washed twice with Lysis buffer, twice with
559 Lysis buffer 500 (Lysis buffer + 360 mM NaCl), twice with Wash buffer (10 mM Tris-HCl pH 8.0,
560 250 mM LiCl, 0.5% NP40, 0.5% Na-deoxycholate, 1 mM EDTA) and once with TE (10 mM Tris-
561 HCl pH 8.0, 1 mM EDTA). Input and immunoprecipitated chromatin were eluted and reverse-
562 crosslinked with 50 µL TE/SDS (TE + 1% SDS) by incubating overnight at 65°C. Samples were
563 treated with RNase A (345 µL TE, 3 µL 10 mg/mL RNAse A (Sigma-Aldrich, R6513), 2 µL 20
564 mg/mL Glycogen (Roche, 10901393001)) at 37°C for 2 hr and subsequently subjected to
565 Proteinase K (15 µL 10% SDS, 7.5 µL 20 mg/mL Proteinase K (Thermo Fisher Scientific,
566 25530049)) digestion at 37°C for 2 hr. Samples were extracted twice with
567 phenol/chloroform/isoamyl alcohol (25:24:1), followed by precipitation with 200 mM NaCl and
568 70% ethanol. Precipitated DNA was resuspended in 50 µL of TE before being used in ChIP-seq
569 libraries.
570 All ChIP and Input samples were subjected to a 1.7X cleanup using KAPA Pure Beads
571 (Roche, 07983280001) according to the manufacturer's instructions. Samples were eluted with
572 40 µL of Elution buffer (10 mM Tris pH 8.0). DNA concentration of ChIP and Input samples was
573 determined by qPCR using a standard curve made with a fragment size control sample. 1-10 ng
574 of ChIP and Input DNA were used for ChIP-seq library preparation as follows. The ends of DNA
575 were repaired by incubating in 70 µL of 1X NEBuffer 2 containing 0.6 units of T4 DNA
576 polymerase (NEB, M0203S), 2 units of T4 polynucleotide kinase (NEB, M0201S), 0.09 nM dNTPs
577 and 0.045 µg/µL of BSA at 12°C for 30 min. Repaired DNA was then subjected to a 1.7X cleanup
578 using KAPA Pure Beads before dA tailing as follows. Beads containing the repaired DNA were
579 resuspended in 50 µL of 1X NEBuffer 2 containing 0.1 mM dATP and 25 units of Klenow
580 Fragment (3'→5' exo-) (NEB, M0212M), and incubated at 37°C for 30 min. After a 1.8X cleanup
581 with KAPA Pure Beads, the A-tailed DNA was ligated to index adapters (Illumina Truseq DNA UD
582 Indexes (20023784)) as follows. The beads were resuspended in 45 µL of 1X Ligase buffer

583 containing 8 nM of adapter and 2.5 units of T4 DNA ligase (ThermoFisher, 15224041) and
584 incubated at room temperature for 60 min. The ligated DNA was then subjected to a 1X
585 cleanup with KAPA Pure Beads, followed by a double size selection (0.52X-1X) leading to
586 fragments in the 200-600 bp range. Libraries were PCR-amplified with 12-13 cycles using KOD
587 Hot Start DNA polymerase (Millipore, 71086-3) and cleaned up using 1X KAPA Pure Beads.
588 Libraries were qualified on Agilent 2100 Bioanalyzer using High Sensitivity DNA Kit and
589 quantified by qPCR using NEBNext Library Quant Kit for Illumina (NEB, E7630). Equal molarity of
590 each library was pooled and subjected to sequencing on Illumina NovaSeq 6000 platform at the
591 McGill University and Génome Québec Innovation Centre to generate 100 bp paired-end reads.
592 **ChIP-seq Data analysis**. ChIP-seq data was analyzed as previously described (Jeronimo
593 et al., 2021). Adapter sequences were removed from paired-end reads for each biological
594 replicate using Trimmomatic, version 0.36 (Bolger et al., 2014) with parameters
595 "ILLUMINACLIP:adapters.fa:2:30:10: TRAILING:3 MINLEN:25". Paired-end reads for each
596 biological replicate were independently aligned to the *S. cerevisiae* (UCSC sacCer3) and *S.*
597 *pombe* (Downloaded from https://www.pombase.org/ on December 7th 2022) reference
598 genomes using the short read aligner Bowtie 2 (version 2.3.4.3) (Langmead et al., 2009). Only
599 reads mapped in proper pairs and primary alignments were kept in aligned files using Samtools,
600 version 1.9 (Li et al., 2009) with parameters "-F 2048 -F 256 -f 2". Duplicate reads were
601 removed from aligned files using Samtools "fixmate" and "markdup -r". Coverage for each base
602 pair of the *S. cerevisiae* genome was computed using genomeCoverageBed from BEDTools,
603 version 2.27.1 (Quinlan & Hall, 2010) and normalized using *S. pombe* reads as follows. The read
604 density at each position of the *S. cerevisiae* genome was multiplied by a normalization factor N
605 defined as:
606
607 $N = 1{,}000{,}000 * P / R * C$
608 where:
609 1,000,000 is an arbitrarily chosen number used for convenience;
610 *R* is the total number of reads in the IP sample that mapped to the *S. pombe* genome;
611 *C* is the total number of reads in the Input sample that mapped to the *S. cerevisiae*
612 genome;
613 *P* is the total number of reads in the Input sample that mapped to the *S. pombe* genome.
614
615 The deduplicated BAM files of replicates were merged using Samtools "merge".
616 Correlation between replicates were generated using deepTools, version 3.5.1 (Ramirez
617 et al., 2016) with parameters "multiBigwigSummary bins --binSize 100" and "plotCorrelation --
618 corMethod pearson --whatToPlot heatmap --colorMap PiYG --plotNumbers".
619 The genome coverage files were converted to the bigWig format using the utilities from
620 UCSC Genome Browser (Casper et al., 2018).
621 Statistics regarding the reads (including the number of reads, mapped reads, the
622 correlation between replicates, etc.) are shown in **Supplemental Table S3**.
623 The RNApII-adjusted Ser5P coverage file (used in **Figure 5E** and **Figure 5 – figure**
624 **supplement 1E**) was generated as follows, starting from *S. pombe*-normalized coverage files.
625 For each genomic position, the Ser5P occupancy value of a given Tfb3 mutant was multiplied by
626 the RNApII occupancy value in WT and divided by the RNApII occupancy value in the mutant.

627 Aggregate profiles (metagene analyses) were generated using the Versatile Aggregate
628 Profiler (VAP) (Brunelle et al., 2015; Coulombe et al., 2014). The aggregate profiles were
629 generated by aligning data on the transcription start site (TSS) and the polyadenylation (pA)
630 signal of all verified genes that have a signal of RNApII >4 and are longer than 1 kb (n=95). The
631 data were averaged over 10 bp bins. TSS and pA site coordinates were from Pelechano et al.
632 (Pelechano et al., 2013).
633 In **Figure 5 – figure supplement 1E**, the values for "promoters" are the average signal
634 over a 200 bp window centered on the TSS whereas the values for "ORFs" are the average of
635 the signal between position +200 and the pA site. The region between +100 and +200 was
636 excluded to avoid signal contamination from promoters for ORFs and vice versa. In **Figure 5 –**
637 **figure supplement 4**, gene classifications are from (Donczew et al., 2020).
638 All raw and processed ChIP-seq data generated in this study have been deposited in the
639 NCBI Gene Expression Omnibus (GEO; http://www.ncbi.nlm.nih.gov/geo/) under accession
640 number GSE241436.
641 **UV sensitivity assay:** Yeast strains were grown in liquid media selective for the *TFB3*
642 plasmids, and overnight cultures were diluted to an OD_{600} = 0.005 and 0.0005 for plating. For
643 each test plate, 100 μL of diluted cells were spread on selective media. Plated cells were then
644 exposed to one of four doses of UV radiation: 0, 30, 60, or 90 J/m^2. UV intensity was calibrated
645 using a UVX Radiometer UVP and dosage calculated by varying time of exposure to a short-
646 wave UV transilluminator. After irradiation, plates were grown at 30°C for 2 days in the dark to
647 avoid photoreactivation repair, and then at room temperature for 5 days. Individual colonies
648 were counted and fraction survivals were calculated and plotted.
649
650
651
652

653 **REFERENCES**

654

655 Abril-Garrido, J., Dienemann, C., Grabbe, F., Velychko, T., Lidschreiber, M., Wang, H., & Cramer,
656 P. (2023). Structural basis of transcription reduction by a promoter-proximal +1
657 nucleosome. *Mol Cell*, *83*(11), 1798-1809 e1797.
658 https://doi.org/10.1016/j.molcel.2023.04.011
659 Badjatia, N., Ambrosio, D. L., Lee, J. H., & Gunzl, A. (2013). Trypanosome cdc2-related kinase 9
660 controls spliced leader RNA cap4 methylation and phosphorylation of RNA polymerase II
661 subunit RPB1. *Mol Cell Biol*, *33*(10), 1965-1975. https://doi.org/10.1128/MCB.00156-13
662 Bataille, A. R., Jeronimo, C., Jacques, P.-E., Laramée, L., Fortin, M.-È., Forest, A., Bergeron, M.,
663 Hanes, S. D., & Robert, F. (2012). A universal RNA polymerase II CTD cycle is
664 orchestrated by complex interplays between kinase, phosphatase, and isomerase
665 enzymes along genes. *Molecular Cell*, *45*(2), 158-170.
666 https://doi.org/10.1016/j.molcel.2011.11.024
667 Bolger, A. M., Lohse, M., & Usadel, B. (2014). Trimmomatic: a flexible trimmer for Illumina
668 sequence data. *Bioinformatics*, *30*(15), 2114-2120.
669 https://doi.org/10.1093/bioinformatics/btu170
670 Brunelle, M., Coulombe, C., Poitras, C., Robert, M. A., Markovits, A. N., Robert, F., & Jacques, P.
671 E. (2015). Aggregate and Heatmap Representations of Genome-Wide Localization Data
672 Using VAP, a Versatile Aggregate Profiler. *Methods Mol Biol*, *1334*, 273-298.
673 https://doi.org/10.1007/978-1-4939-2877-4_18
674 Buratowski, S. (2009). Progression through the RNA polymerase II CTD cycle. *Mol Cell*, *36*(4),
675 541-546. https://doi.org/10.1016/j.molcel.2009.10.019
676 Callebaut, I., Prat, K., Meurice, E., Mornon, J. P., & Tomavo, S. (2005). Prediction of the general
677 transcription factors associated with RNA polymerase II in Plasmodium falciparum:
678 conserved features and differences relative to other eukaryotes. *BMC genomics*, *6*, 100.
679 https://doi.org/10.1186/1471-2164-6-100
680 Casper, J., Zweig, A. S., Villarreal, C., Tyner, C., Speir, M. L., Rosenbloom, K. R., Raney, B. J., Lee,
681 C. M., Lee, B. T., Karolchik, D., Hinrichs, A. S., Haeussler, M., Guruvadoo, L., Navarro
682 Gonzalez, J., Gibson, D., Fiddes, I. T., Eisenhart, C., Diekhans, M., Clawson, H.,…Kent, W.
683 J. (2018). The UCSC Genome Browser database: 2018 update. *Nucleic Acids Res*, *46*(D1),
684 D762-D769. https://doi.org/10.1093/nar/gkx1020
685 Chapman, R. D., Heidemann, M., Albert, T. K., Mailhammer, R., Flatley, A., Meisterernst, M.,
686 Kremmer, E., & Eick, D. (2007). Transcribing RNA polymerase II is phosphorylated at CTD
687 residue serine-7. *Science (New York, NY)*, *318*(5857), 1780-1782.
688 https://doi.org/10.1126/science.1145977
689 Chen, X., Qi, Y., Wu, Z., Wang, X., Li, J., Zhao, D., Hou, H., Li, Y., Yu, Z., Liu, W., Wang, M., Ren, Y.,
690 Li, Z., Yang, H., & Xu, Y. (2021). Structural insights into preinitiation complex assembly on
691 core promoters. *Science*, *372*(6541). https://doi.org/10.1126/science.aba8490
692 Chen, Y., Jirage, D., Caridha, D., Kathcart, A. K., Cortes, E. A., Dennull, R. A., Geyer, J. A., Prigge,
693 S. T., & Waters, N. C. (2006). Identification of an effector protein and gain-of-function
694 mutants that activate Pfmrk, a malarial cyclin-dependent protein kinase. *Mol Biochem*
695 *Parasitol*, *149*(1), 48-57. https://doi.org/10.1016/j.molbiopara.2006.04.004

696 Cho, E. J., Kobor, M. S., Kim, M., Greenblatt, J., & Buratowski, S. (2001). Opposing effects of Ctk1
697 kinase and Fcp1 phosphatase at Ser 2 of the RNA polymerase II C-terminal domain.
698 *Genes and Development*, *15*(24), 3319-3329. https://doi.org/10.1101/gad.935901
699 Chun, Y., Joo, Y. J., Suh, H., Batot, G., Hill, C. P., Formosa, T., & Buratowski, S. (2019). Selective
700 Kinase Inhibition Shows That Bur1 (Cdk9) Phosphorylates the Rpb1 Linker In Vivo. *Mol*
701 *Cell Biol*, *39*(15), e00602-00618. https://doi.org/10.1128/MCB.00602-18
702 Cismowski, M. J., Laff, G. M., Solomon, M. J., & Reed, S. I. (1995). KIN28 encodes a C-terminal
703 domain kinase that controls mRNA transcription in Saccharomyces cerevisiae but lacks
704 cyclin-dependent kinase-activating kinase (CAK) activity. *Mol Cell Biol*, *15*(6), 2983-2992.
705 https://doi.org/10.1128/MCB.15.6.2983
706 Corden, J. L. (2013). RNA polymerase II C-terminal domain: Tethering transcription to transcript
707 and template. [Review]. *Chemical reviews*, *113*(11), 8423-8455.
708 https://doi.org/10.1021/cr400158h
709 Coulombe, C., Poitras, C., Nordell-Markovits, A., Brunelle, M., Lavoie, M. A., Robert, F., &
710 Jacques, P. E. (2014). VAP: a versatile aggregate profiler for efficient genome-wide data
711 representation and discovery. *Nucleic Acids Res*, *42*(Web Server issue), W485-493.
712 https://doi.org/10.1093/nar/gku302
713 Das, A., & Bellofatto, V. (2009). The non-canonical CTD of RNAP-II is essential for productive
714 RNA synthesis in Trypanosoma brucei. *PLoS ONE*, *4*(9), e6959.
715 https://doi.org/10.1371/journal.pone.0006959
716 Donczew, R., Warfield, L., Pacheco, D., Erijman, A., & Hahn, S. (2020). Two roles for the yeast
717 transcription coactivator SAGA and a set of genes redundantly regulated by TFIID and
718 SAGA. *eLife*, *9*. https://doi.org/10.7554/eLife.50109
719 Eick, D., & Geyer, M. (2013). The RNA polymerase II carboxy-terminal domain (CTD) code.
720 [Review]. *Chemical reviews*, *113*(11), 8456-8490. https://doi.org/10.1021/cr400071f
721 Espinoza, F. H., Farrell, A., Erdjument-Bromage, H., Tempst, P., & Morgan, D. O. (1996). A cyclin-
722 dependent kinase-activating kinase (CAK) in budding yeast unrelated to vertebrate CAK.
723 *Science*, *273*(5282), 1714-1717. https://doi.org/10.1126/science.273.5282.1714
724 Feaver, W. J., Huang, W., Gileadi, O., Myers, L., Gustafsson, C. M., Kornberg, R. D., & Friedberg,
725 E. C. (2000). Subunit interactions in yeast transcription/repair factor TFIIH. Requirement
726 for Tfb3 subunit in nucleotide excision repair. *Journal of Biological Chemistry*, *275*(8),
727 5941-5946. https://doi.org/10.1074/jbc.275.8.5941
728 Fisher, R. P., & Morgan, D. O. (1994). A novel cyclin associates with MO15/CDK7 to form the
729 CDK-activating kinase. *Cell*, *78*(4), 713-724. https://doi.org/10.1016/0092-
730 8674(94)90535-5
731 Glover-Cutter, K., Larochelle, S., Erickson, B., Zhang, C., Shokat, K., Fisher, R. P., & Bentley, D. L.
732 (2009). TFIIH-associated Cdk7 kinase functions in phosphorylation of C-terminal domain
733 Ser7 residues, promoter-proximal pausing, and termination by RNA polymerase II.
734 *Molecular and Cellular Biology*, *29*(20), 5455-5464. https://doi.org/10.1128/MCB.00637-
735 09
736 Greber, B. J., Perez-Bertoldi, J. M., Lim, K., Iavarone, A. T., Toso, D. B., & Nogales, E. (2020). The
737 cryoelectron microscopy structure of the human CDK-activating kinase. *Proc Natl Acad*
738 *Sci U S A*, *117*(37), 22849-22857. https://doi.org/10.1073/pnas.2009627117

739 Greber, B. J., Toso, D. B., Fang, J., & Nogales, E. (2019). The complete structure of the human
740 TFIIH core complex. *eLife*, *8*, E633. https://doi.org/10.7554/eLife.44771
741 Grünberg, S., Warfield, L., & Hahn, S. (2012). Architecture of the RNA polymerase II preinitiation
742 complex and mechanism of ATP-dependent promoter opening. *Nature structural &*
743 *molecular biology*, *19*(8), 788-796. https://doi.org/10.1038/nsmb.2334
744 Guo, Z., & Stiller, J. W. (2004). Comparative genomics of cyclin-dependent kinases suggest co-
745 evolution of the RNAP II C-terminal domain and CTD-directed CDKs. [Comparative
746 Study]. *BMC genomics*, *5*(1), 69. https://doi.org/10.1186/1471-2164-5-69
747 Guo, Z., & Stiller, J. W. (2005). Comparative genomics and evolution of proteins associated with
748 RNA polymerase II C-terminal domain. [Comparative Study]. *Molecular Biology and*
749 *Evolution*, *22*(11), 2166-2178. https://doi.org/10.1093/molbev/msi215
750 Harlow, E., & Lane, D. P. (1988). *Antibodies: A Laboratory Manual*. Cold Spring Harbor
751 Laboratory Press, Inc.
752 He, Y., Yan, C., Fang, J., Inouye, C., Tjian, R., Ivanov, I., & Nogales, E. (2016). Near-atomic
753 resolution visualization of human transcription promoter opening. *Nature*, *533*(7603),
754 359-365. https://doi.org/10.1038/nature17970
755 Helenius, K., Yang, Y., Tselykh, T. V., Pessa, H. K. J., Frilander, M. J., & Mäkelä, T. P. (2011).
756 Requirement of TFIIH kinase subunit Mat1 for RNA Pol II C-terminal domain Ser5
757 phosphorylation, transcription and mRNA turnover. *Nucleic Acids Research*, *39*(12),
758 5025-5035. https://doi.org/10.1093/nar/gkr107
759 Jeronimo, C., Angel, A., Nguyen, V. Q., Kim, J. M., Poitras, C., Lambert, E., Collin, P., Mellor, J.,
760 Wu, C., & Robert, F. (2021). FACT is recruited to the +1 nucleosome of transcribed genes
761 and spreads in a Chd1-dependent manner. *Mol Cell*.
762 https://doi.org/10.1016/j.molcel.2021.07.010
763 Jeronimo, C., Poitras, C., & Robert, F. (2019). Histone Recycling by FACT and Spt6 during
764 Transcription Prevents the Scrambling of Histone Modifications. *Cell reports*, *28*(5),
765 1206-1218.e1208. https://doi.org/10.1016/j.celrep.2019.06.097
766 Jeronimo, C., & Robert, F. (2014). Kin28 regulates the transient association of Mediator with
767 core promoters. *Nature Structural & Molecular Biology*, *21*(5), 449-455.
768 https://doi.org/10.1038/nsmb.2810
769 Joo, Y. J., Ficarro, S. B., Chun, Y., Marto, J. A., & Buratowski, S. (2019). In vitro analysis of RNA
770 polymerase II elongation complex dynamics. *Genes and Development*, *33*(9-10), 578-
771 589. https://doi.org/10.1101/gad.324202.119
772 Kaldis, P., Sutton, A., & Solomon, M. J. (1996). The Cdk-activating kinase (CAK) from budding
773 yeast. *Cell*, *86*(4), 553-564. https://doi.org/10.1016/s0092-8674(00)80129-4
774 Keogh, M. C., Cho, E. J., Podolny, V., & Buratowski, S. (2002). Kin28 is found within TFIIH and a
775 Kin28-Ccl1-Tfb3 trimer complex with differential sensitivities to T-loop phosphorylation.
776 *Mol Cell Biol*, *22*(5), 1288-1297. https://doi.org/10.1128/MCB.22.5.1288-1297.2002
777 Keogh, M. C., Podolny, V., & Buratowski, S. (2003). Bur1 kinase is required for efficient
778 transcription elongation by RNA polymerase II. *Mol Cell Biol*, *23*(19), 7005-7018.
779 https://doi.org/10.1128/MCB.23.19.7005-7018.2003
780 Kim, J., Li, C. L., Chen, X., Cui, Y., Golebiowski, F. M., Wang, H., Hanaoka, F., Sugasawa, K., &
781 Yang, W. (2023). Lesion recognition by XPC, TFIIH and XPA in DNA excision repair.
782 *Nature*, *617*(7959), 170-175. https://doi.org/10.1038/s41586-023-05959-z

783 Komarnitsky, P., Cho, E. J., & Buratowski, S. (2000). Different phosphorylated forms of RNA
784 polymerase II and associated mRNA processing factors during transcription. *Genes Dev*,
785 *14*(19), 2452-2460. https://doi.org/10.1101/gad.824700
786 Kuldell, N. H., & Buratowski, S. (1997). Genetic analysis of the large subunit of yeast
787 transcription factor IIE reveals two regions with distinct functions. *Mol Cell Biol*, *17*(9),
788 5288-5298. https://doi.org/10.1128/MCB.17.9.5288
789 Kushnirov, V. V. (2000). Rapid and reliable protein extraction from yeast. *Yeast*, *16*(9), 857-860.
790 https://doi.org/10.1002/1097-0061(20000630)16:9<857::AID-YEA561>3.0.CO;2-B
791 Langmead, B., Trapnell, C., Pop, M., & Salzberg, S. L. (2009). Ultrafast and memory-efficient
792 alignment of short DNA sequences to the human genome. [OriginalPaper]. *Genome*
793 *biology*, *10*(3), R25. https://doi.org/10.1186/gb-2009-10-3-r25
794 Lee, J. H., Cai, G., Panigrahi, A. K., Dunham-Ems, S., Nguyen, T. N., Radolf, J. D., Asturias, F. J., &
795 Gunzl, A. (2010). A TFIIH-Associated Mediator Head Is a Basal Factor of Small Nuclear
796 Spliced Leader RNA Gene Transcription in Early-Diverged Trypanosomes. *Molecular and*
797 *Cellular Biology*, *30*(23), 5502-5513. https://doi.org/10.1128/MCB.00966-10
798 Lee, J. H., Jung, H. S., & Günzl, A. (2009). Transcriptionally active TFIIH of the early-diverged
799 eukaryote Trypanosoma brucei harbors two novel core subunits but not a cyclin-
800 activating kinase complex. *Nucleic Acids Research*, *37*(11), 3811-3820.
801 https://doi.org/10.1093/nar/gkp236
802 Li, H., Handsaker, B., Wysoker, A., Fennell, T., Ruan, J., Homer, N., Marth, G., Abecasis, G.,
803 Durbin, R., & Subgroup, G. P. D. P. (2009). The Sequence Alignment/Map format and
804 SAMtools. *Bioinformatics (Oxford, England)*, *25*(16), 2078-2079.
805 https://doi.org/10.1093/bioinformatics/btp352
806 Matsui, P., DePaulo, J., & Buratowski, S. (1995). An interaction between the Tfb1 and Ssl1
807 subunits of yeast TFIIH correlates with DNA repair activity. *Nucleic Acids Res*, *23*(5), 767-
808 772. https://doi.org/10.1093/nar/23.5.767
809 Mayer, A., Lidschreiber, M., Siebert, M., Leike, K., Soding, J., & Cramer, P. (2010). Uniform
810 transitions of the general RNA polymerase II transcription complex. *Nat Struct Mol Biol*,
811 *17*(10), 1272-1278. https://doi.org/10.1038/nsmb.1903
812 Murakami, K., Gibbons, B. J., Davis, R. E., Nagai, S., Liu, X., Robinson, P. J. J., Wu, T., Kaplan, C.
813 D., & Kornberg, R. D. (2012). Tfb6, a previously unidentified subunit of the general
814 transcription factor TFIIH, facilitates dissociation of Ssl2 helicase after transcription
815 initiation. *Proceedings of the National Academy of Sciences of the United States of*
816 *America*, *109*(13), 4816-4821. https://doi.org/10.1073/pnas.1201448109
817 Murakami, K., Mattei, P. J., Davis, R. E., Jin, H., Kaplan, C. D., & Kornberg, R. D. (2015).
818 Uncoupling Promoter Opening from Start-Site Scanning. *Mol Cell*, *59*(1), 133-138.
819 https://doi.org/10.1016/j.molcel.2015.05.021
820 Nguyen, V. Q., Ranjan, A., Liu, S., Tang, X., Ling, Y. H., Wisniewski, J., Mizuguchi, G., Li, K. Y., Jou,
821 V., Zheng, Q., Lavis, L. D., Lionnet, T., & Wu, C. (2021). Spatiotemporal coordination of
822 transcription preinitiation complex assembly in live cells. *Mol Cell*, *81*(17), 3560-3575
823 e3566. https://doi.org/10.1016/j.molcel.2021.07.022
824 Peissert, S., Schlosser, A., Kendel, R., Kuper, J., & Kisker, C. (2020). Structural basis for CDK7
825 activation by MAT1 and Cyclin H. *Proc Natl Acad Sci U S A*, *117*(43), 26739-26748.
826 https://doi.org/10.1073/pnas.2010885117

827 Pelechano, V., Wei, W., & Steinmetz, L. M. (2013). Extensive transcriptional heterogeneity
828 revealed by isoform profiling. *Nature*, *497*(7447), 127-131.
829 https://doi.org/10.1038/nature12121
830 Quinlan, A. R., & Hall, I. M. (2010). BEDTools: a flexible suite of utilities for comparing genomic
831 features. *Bioinformatics*, *26*(6), 841-842. https://doi.org/10.1093/bioinformatics/btq033
832 Ramirez, F., Ryan, D. P., Gruning, B., Bhardwaj, V., Kilpert, F., Richter, A. S., Heyne, S., Dundar,
833 F., & Manke, T. (2016). deepTools2: a next generation web server for deep-sequencing
834 data analysis. *Nucleic Acids Res*, *44*(W1), W160-165.
835 https://doi.org/10.1093/nar/gkw257
836 Rimel, J. K., Poss, Z. C., Erickson, B., Maas, Z. L., Ebmeier, C. C., Johnson, J. L., Decker, T. M.,
837 Yaron, T. M., Bradley, M. J., Hamman, K. B., Hu, S., Malojcic, G., Marineau, J. J., White, P.
838 W., Brault, M., Tao, L., DeRoy, P., Clavette, C., Nayak, S.,…Taatjes, D. J. (2020). Selective
839 inhibition of CDK7 reveals high-confidence targets and new models for TFIIH function in
840 transcription. *Genes Dev*, *34*(21-22), 1452-1473.
841 https://doi.org/10.1101/gad.341545.120
842 Robinson, P. J., Trnka, M. J., Bushnell, D. A., Davis, R. E., Mattei, P.-J., Burlingame, A. L., &
843 Kornberg, R. D. (2016). Structure of a Complete Mediator-RNA Polymerase II Pre-
844 Initiation Complex. *Cell*, *166*(6), 1411-1414.e1416.
845 https://doi.org/10.1016/j.cell.2016.08.050
846 Sano, M., Izumi, Y., Helenius, K., Asakura, M., Rossi, D. J., Xie, M., Taffet, G., Hu, L., Pautler, R.
847 G., Wilson, C. R., Boudina, S., Abel, E. D., Taegtmeyer, H., Scaglia, F., Graham, B. H.,
848 Kralli, A., Shimizu, N., Tanaka, H., Makela, T. P., & Schneider, M. D. (2007). Menage-a-
849 trois 1 is critical for the transcriptional function of PPARgamma coactivator 1. *Cell*
850 *Metab*, *5*(2), 129-142. https://doi.org/10.1016/j.cmet.2007.01.003
851 Schier, A. C., & Taatjes, D. J. (2021). Everything at once: cryo-EM yields remarkable insights into
852 human RNA polymerase II transcription. *Nat Struct Mol Biol*, *28*(7), 540-543.
853 https://doi.org/10.1038/s41594-021-00613-6
854 Schilbach, S., Hantsche, M., Tegunov, D., Dienemann, C., Wigge, C., Urlaub, H., & Cramer, P.
855 (2017). Structures of transcription pre-initiation complex with TFIIH and Mediator.
856 *Nature*, *551*(7679), 204-209. https://doi.org/10.1038/nature24282
857 Schilbach, S., Wang, H., Dienemann, C., & Cramer, P. (2023). Yeast PIC-Mediator structure with
858 RNA polymerase II C-terminal domain. *Proc Natl Acad Sci U S A*, *120*(15), e2220542120.
859 https://doi.org/10.1073/pnas.2220542120
860 Sogaard, T. M., & Svejstrup, J. Q. (2007). Hyperphosphorylation of the C-terminal repeat
861 domain of RNA polymerase II facilitates dissociation of its complex with mediator. *J Biol*
862 *Chem*, *282*(19), 14113-14120. https://doi.org/10.1074/jbc.M701345200
863 Suh, H., Ficarro, S. B., Kang, U.-B., Chun, Y., Marto, J. A., & Buratowski, S. (2016). Direct Analysis
864 of Phosphorylation Sites on the Rpb1 C-Terminal Domain of RNA Polymerase II.
865 *Molecular Cell*, *61*(2), 297-304. https://doi.org/10.1016/j.molcel.2015.12.021
866 Sung, P., Higgins, D., Prakash, L., & Prakash, S. (1988). Mutation of lysine-48 to arginine in the
867 yeast RAD3 protein abolishes its ATPase and DNA helicase activities but not the ability to
868 bind ATP. *EMBO J*, *7*(10), 3263-3269. https://doi.org/10.1002/j.1460-
869 2075.1988.tb03193.x

870 Thomas, M. C., & Chiang, C. M. (2006). The general transcription machinery and general
871 cofactors [Review]. *Critical reviews in biochemistry and molecular biology*, *41*(3), 105-
872 178. https://doi.org/10.1080/10409230600648736
873 Tietjen, J. R., Zhang, D. W., Rodriguez-Molina, J. B., White, B. E., Akhtar, M. S., Heidemann, M.,
874 Li, X., Chapman, R. D., Shokat, K., Keles, S., Eick, D., & Ansari, A. Z. (2010). Chemical-
875 genomic dissection of the CTD code. *Nat Struct Mol Biol*, *17*(9), 1154-1161.
876 https://doi.org/10.1038/nsmb.1900
877 Tomko, E. J., Luyties, O., Rimel, J. K., Tsai, C. L., Fuss, J. O., Fishburn, J., Hahn, S., Tsutakawa, S.
878 E., Taatjes, D. J., & Galburt, E. A. (2021). The Role of XPB/Ssl2 dsDNA Translocase
879 Processivity in Transcription Start-site Scanning. *J Mol Biol*, *433*(14), 166813.
880 https://doi.org/10.1016/j.jmb.2021.166813
881 van Eeuwen, T., Li, T., Kim, H. J., Gorbea Colon, J. J., Parker, M. I., Dunbrack, R. L., Garcia, B. A.,
882 Tsai, K. L., & Murakami, K. (2021). Structure of TFIIK for phosphorylation of CTD of RNA
883 polymerase II. *Sci Adv*, *7*(15). https://doi.org/10.1126/sciadv.abd4420
884 van Eeuwen, T., Shim, Y., Kim, H. J., Zhao, T., Basu, S., Garcia, B. A., Kaplan, C. D., Min, J. H., &
885 Murakami, K. (2021). Cryo-EM structure of TFIIH/Rad4-Rad23-Rad33 in damaged DNA
886 opening in nucleotide excision repair. *Nat Commun*, *12*(1), 3338.
887 https://doi.org/10.1038/s41467-021-23684-x
888 van Sluis, M., Gonzalo-Hansen, C., Li, Q., Lans, H., Wang, D., & Marteijn, J. A. (2025).
889 Mechanisms of transcription-coupled repair and DNA damage surveillance in health and
890 disease. *Nat Rev Mol Cell Biol*. https://doi.org/10.1038/s41580-025-00915-3
891 Vannini, A., & Cramer, P. (2012). Conservation between the RNA Polymerase I, II, and III
892 Transcription Initiation Machineries. *Molecular Cell*, *45*(4), 439-446.
893 https://doi.org/10.1016/j.molcel.2012.01.023
894 Warfield, L., Luo, J., Ranish, J., & Hahn, S. (2016). Function of Conserved Topological Regions
895 within the Saccharomyces cerevisiae Basal Transcription Factor TFIIH. *Molecular and*
896 *Cellular Biology*, *36*(19), 2464-2475. https://doi.org/10.1128/MCB.00182-16
897 Watanabe, T., Hayashi, K., Tanaka, A., Furumoto, T., Hanaoka, F., & Ohkuma, Y. (2003). The
898 carboxy terminus of the small subunit of TFIIE regulates the transition from transcription
899 initiation to elongation by RNA polymerase II [In Vitro]. *Molecular and Cellular Biology*,
900 *23*(8), 2914-2926.
901 http://mcb.asm.org/cgi/content/full/23/8/2914?view=long&pmid=12665589
902 Winkler, G. S., Araujo, S. J., Fiedler, U., Vermeulen, W., Coin, F., Egly, J. M., Hoeijmakers, J. H.,
903 Wood, R. D., Timmers, H. T., & Weeda, G. (2000). TFIIH with inactive XPD helicase
904 functions in transcription initiation but is defective in DNA repair. *J Biol Chem*, *275*(6),
905 4258-4266. https://doi.org/10.1074/jbc.275.6.4258
906 Wong, K. H., Jin, Y., & Struhl, K. (2014). TFIIH Phosphorylation of the Pol II CTD Stimulates
907 Mediator Dissociation from the Preinitiation Complex and Promoter Escape. *Molecular*
908 *Cell*, *54*(4), 601-612. https://doi.org/10.1016/j.molcel.2014.03.024
909 Yang, C., Fujiwara, R., Kim, H. J., Basnet, P., Zhu, Y., Gorbea Colon, J. J., Steimle, S., Garcia, B. A.,
910 Kaplan, C. D., & Murakami, K. (2022). Structural visualization of de novo transcription
911 initiation by Saccharomyces cerevisiae RNA polymerase II. *Mol Cell*, *82*(3), 660-676 e669.
912 https://doi.org/10.1016/j.molcel.2021.12.020

913 Yu, J., Yan, C., Dodd, T., Tsai, C. L., Tainer, J. A., Tsutakawa, S. E., & Ivanov, I. (2023). Dynamic
914 conformational switching underlies TFIIH function in transcription and DNA repair and
915 impacts genetic diseases. *Nat Commun*, *14*(1), 2758. https://doi.org/10.1038/s41467-
916 023-38416-6
917 Yurko, N., Liu, X., Yamazaki, T., Hoque, M., Tian, B., & Manley, J. L. (2017). MPK1/SLT2 Links
918 Multiple Stress Responses with Gene Expression in Budding Yeast by Phosphorylating
919 Tyr1 of the RNAP II CTD. *Molecular Cell*, *68*(5), 913-925.e913.
920 https://doi.org/10.1016/j.molcel.2017.11.020
921
922

923 **Figure Legends**
924
925 **Figure 1. Tfb3 N-term-Linker fusions to other kinase modules can replace Tfb3, but not Kin28.**
926 **(A)** Schematic of TFIIH structure within the PIC. The domain structure of Tfb3 (green) is shown,
927 connecting the TFIIH Kinase (cyan) and Core (blue) Modules. **(B)** Schematic of Tfb3 fusions to
928 other kinase modules. **(C)** The *kin28Δ* strain YSB744 was transformed with pRS425 (Vector),
929 pRS415-*KIN28*, pRS425-*TFB3-BUR2*, pRS425-*TFB3-CTK3*, or pRS425-*TFB3-MPK1*. Transformants
930 were tested for the ability to replace a *KIN28/URA3* construct by plasmid shuffling. Cells were
931 streaked on -LEU-TRP (center) or -LEU-TRP+5-FOA (right) plates for 3 days at 30℃. **(D)** pRS315
932 (Vector), pRS425-*TFB3*, pRS315/TFB3Δ2 (aa 1-275) (Feaver et al., 2000), pRS425-*TFB3-BUR2*,
933 pRS425-*TFB3-CTK3*, and pRS425-*TFB3-MPK1* were transformed into *tfb3Δ* strain SHY907
934 (Warfield et al., 2016), replacing the plasmid-expressed wild-type gene by plasmid shuffling.
935 Streaks shown were grown on –LEU for 4 days (center) or on -LEU+5-FOA plates (right) for 9
936 days.
937
938 **Figure 2. Tfb3 can be split into two functional parts.**
939 **(A)** Schematic of Tfb3 deletion constructs. Note that all constructs retained amino acids 1-11 at
940 the N-terminus for ease of cloning and to avoid differential sensitivity to N-end rule
941 degradation. **(B)** Plasmid shuffling was used to test pRS424 (Vector), pRS424-*TFB3* (WT *TFB3*),
942 pRS424-*TFB3(*Δ145-321) (N-term), and pRS424-*TFB3* (Δ252-321) (N-term-Linker) for the ability
943 to support growth of *tfb3Δ* shuffling strain SHY907/YF2456 (Warfield et al., 2016). Streaks
944 shown were grown on -TRP+5-FOA plates for 5 days at 30℃ **(C)** Spot assay for growth. Tfb3 N-
945 term (YSB3704) and N-term-Linker (YSB3722) strains were transformed with pRS425 (Vector),
946 pSH1542 (WT *TFB3*), pRS315-TFB3(1-11, 238-Stop)-Flag1-TAP (C-term low copy), pRS425-
947 TFB3(1-11, 238-Stop) (C-term high copy), pRS425-TFB3(1-11, 139-Stop) (Linker-C-term low
948 copy), or pLH366 (Linker-C-term high copy). Ten-fold serial dilutions were spotted onto –LEU-
949 TRP plates for 3 days. For comparison to normal growth, an isogenic strain carrying WT *TFB3*
950 (YSB3788) was spotted in parallel (top strip).
951
952 **Figure 3. The TFIIH Kinase Module associates with the untethered Tfb3 C-terminal domain. (A)**
953 Whole cell extracts were made from YSB3788 (*TFB3* untagged), YSB3723 (*TFB3*-TAP + N-term),
954 YSB3732 (N-term-Linker + C-term-TAP), and YSB3728 (N-term + Linker-C-term-TAP). Both Input
955 extracts (lanes 1-4) and IgG-Agarose precipitated fractions (lanes 5-8) were resolved by SDS-
956 PAGE and blotting for Tfb3. **(B)** To probe for other Kinase Module subunits, IgG precipitates
957 were probed with anti-Ccl1 and anti-Kin28 antibodies. In all panels, asterisks mark TAP-tagged
958 Tfb3 derivatives (which also react with secondary antibody due to the protein A component).
959
960 **Figure 4. Splitting Tfb3 uncouples the TFIIH Kinase Module from the Core Module and the PIC.**
961 The same IgG-Agarose precipitates analyzed in **Fig. 3** were also probed with the following
962 antibodies against: **(A)** TFIIH Core Module subunit Tfb1 (note background binding of Tfb1 to
963 beads as seen in lane 1, and non-specific band ~50 kDa), and **(B)** TFIIE subunits Tfa1 and Tfa2
964 (note non-specific band ~60 kDa), which serves as a marker for the RNApII PIC. In all panels,
965 asterisks mark TAP-tagged Tfb3 derivatives reacting with secondary antibody due to the protein
966 A component.

967
968 **Figure 5**. **Loss of proper Kinase Module and Ser5P promoter localization in split Tfb3 cells**.
969 Crosslinked chromatin was prepared from strains expressing full length Tfb3 (YSB3788, red
970 line), the separated N-term-Linker and C-term derivatives (YSB3731, yellow), the N-term and
971 Linker-C-term derivatives (YSB3727, blue), or N-term and C-term with no Linker (YSB3725,
972 green). Samples were immunoprecipitated and processed for sequencing of crosslinked DNA as
973 described in Methods. Two biological replicates for each antibody were used to generate
974 metagene profiles of **(A)** TFIIH Core subunit Tfb1, **(B)** TFIIH Kinase subunit Kin28, **(C)** Rpb1 CTD
975 Ser5P, **(D)** RNApII subunit Rpb1, and **(E)** Ser5P normalized to total Rpb1. The analysis used only
976 those nuclear genes with an average RNApII occupancy greater than 4 reads per million (rpm)
977 and longer than 1 kb (n=95). Individual replicates are shown in **Figure 5 Supplement 1**. To
978 account for the differing lengths of genes, each graph shows 1 kb centered on the transcription
979 start site (TSS) to the left of the dividing line, and 1 kb centered on the polyadenylation site (pA)
980 to the right.
981
982 **Figure 6**. **Split Tfb3 strains are not hyper-sensitive to UV light**. Yeast strains carrying the
983 indicated Tfb3 configurations were plated at various densities and exposed to the indicated
984 dosages of UV light. Surviving colonies were counted after several days. The graph shows the
985 averaged values from multiple replicates, and error bars represent standard deviation. Note
986 that there are two strain backgrounds. The *tfb1-101* strain (YSB250, black) is a positive control
987 for an NER-defective strain sensitive to UV light, and its isogenic WT control is YSB207 (yellow).
988 The other five isogenic strains are in a *tfb6Δ* background (Warfield et al., 2016), lacking the Tfb6
989 protein that competes with the TFIIH for Ssl2 binding (Murakami et al., 2012): WT/tfb6Δ
990 (YSB3788, green), N-term (YSB3724, red), N-term-Linker (YSB3729, blue), N-term + Linker-C-
991 term (YSB3727, orange), and N-term-Linker + C-term (YSB3731, slate).
992
993 **Figure 7. Model for linkage between the TFIIH Kinase and Core Module functions. A.** In free
994 TFIIH, the Tfb3 linker contacts the Ssl2/XPB subunit to create a "closed" conformation. In this
995 configuration, the translocase, and possibly the kinase, may be inhibited. **B.** Upon TFIIH
996 incorporation as the final component of the PIC, the Kinase Module engages with both
997 Mediator (not pictured) and the CTD. These interactions may help release the Tfb3/MAT1 linker
998 from Ssl2/XPB, allowing the translocase to access downstream DNA to promote ATP hydrolysis
999 and promoter melting.
1000
1001
1002

1003 **Figure Supplement Legends**
1004
1005 **Figure 1 – figure supplement 1.** Immunoblot of Tfb3 fusions from **Fig. 1C**. Whole extracts were
1006 made from the post-FOA strains constructed by shuffling pRS425-*TFB3-BUR2*, pRS425-*TFB3-*
1007 *CTK3*, or pRS425-*TFB3-MPK1* into *tfb3Δ* strain SHY907/YF2456 (Warfield et al., 2016). Extracts
1008 were resolved by SDS-PAGE, blotted to a membrane, and probed with anti-Tfb3 antiserum. Left-
1009 most lane shows markers imaged with visible light, and the rest of the blot shows
1010 chemiluminescence detection.
1011
1012 **Figure 3 – figure supplement 1.** Tethered and untethered Kinase Module have similar CTD
1013 kinase specific activity in vitro.
1014 **(A)** Kinase Module was isolated from YSB3707 (TFB3-TAP), YSB3732 (N-term-Linker + C-term-
1015 TAP), and YSB3728 (N-term + Linker-C-term-TAP) using the TAP tag. A parallel isolation from the
1016 untagged strain YSB3788 (WT TFB3) showed that binding was dependent on the TAP tag. The
1017 second lane shows a Kin28-TAP precipitate (not done in parallel) as size marker. Relative levels
1018 of the Kin28 subunit on beads were determined by immunoblotting 8uL, 4uL, and 2uL of beads.
1019 **(B)** In vitro CTD phosphorylation assay. After roughly normalizing bead volumes for amount of
1020 bound Kin28, kinase reactions were performed with GST-CTD. Samples were taken at the
1021 indicated time points and tested for CTD Ser5 phosphorylation using monoclonal antibody 3E8.
1022 Note the phosphorylated CTD as a series of bands, with slower mobility believed to represent
1023 denser phosphorylation. To mark the position of unphosphorylated GST-CTD, a negative control
1024 reaction lane from the blot was probed with 8WG16 (left panel).
1025
1026 **Figure 5 – figure supplement 1.** Additional ChIP-seq analysis. (**A-D**) These panels are the same
1027 metagene analysis as Figure 5A-D, but showing the individual replicates as separate lines. The
1028 Tfb3 configurations are indicated in the key at the bottom: wild-type Tfb3 in reds, N-term-
1029 Linker + C-term in yellows, N-term + Linker-C-term in blues, and N-term + C-term in greens. (**E**)
1030 For each split Tfb3 mutant (color coded as in A-D), a plot of the mutant/WT $\log_2$ RNApII-
1031 adjusted Ser5P ratio versus WT RNApII occupancy, for all verified genes (n=5587), over
1032 promoters (left) and ORFs (right) (see Methods). In panels E and F, the x-axis is cut at 400 rpm
1033 for clarity, excluding only three genes with higher occupancy. (**F**) Plots of the mutant/WT $\log_2$
1034 ratio versus WT level for RNApII occupancy, over ORFs for all verified genes (n=5573). Yellow:
1035 N-term-Linker + C-term, Blue: N-term + Linker-C-term, and Green: N-term + C-term. (**G**)
1036 Heatmap of the mutant/WT $\log_2$ RNApII ratio for the seven genes that are systematically
1037 induced (mutant/WT $\log_2$ RNApII ratio>0) in all three split mutants. All but *ANS1* are known to
1038 be involved in stress-response.
1039
1040 **Figure 5 – figure supplement 2**. Immunoblot for CTD phosphorylation levels in strains with split
1041 Tfb3 or completely lacking the C-term. Whole cell extracts from YSB3712 (WT), YSB3710 (N-
1042 term), YSB 3711 (N-term-Linker), YSB3731 (N-term-Linker + C-term), and YSB3727 (N-term +
1043 Linker-C-term) were resolved by SDS-PAGE and immunoblotted. The top blot shows CTD Ser5P
1044 (monoclonal antibody 3E8), the middle blot shows Ser2P (monoclonal antibody 3E10), and the
1045 bottom blot shows both Rpb1 (monoclonal antibody 8WG16) and Rpb3 (monoclonal antibody
1046 1Y26).

1047
1048 **Figure 5 – figure supplement 3**. Individual gene traces from the ChIP-seq analysis show Ser5P
1049 changes in split Tfb3 strains. **A.** Rpb1 and Ser5P signals at a region containing five strong
1050 promoters (shaded in green) were plotted using the UCSC browser (https://genome.ucsc.edu).
1051 Blue bars above traces show gene locations, with arrows showing direction of transcription.
1052 Numbers in the right-hand corner show the read count scale of the y-axis. **B.** Traces of total
1053 Rpb1, Ser5P, and Ser2P at the strongly transcribed *PMA1* gene. Annotations are as in part A.
1054
1055 **Figure 5 - figure supplement 4**. Effects of Tfb3 split mutants on RNApII occupancy are consistent
1056 across different gene classes. **A.** Metagene analysis of RNApII occupancy at "long" genes, defined
1057 as genes longer than 2 kb and having an average RNApII occupancy greater than 2 reads per
1058 million (rpm) (n=41). **B.** Metagene analysis of RNApII occupancy over all genes longer than 1 kb
1059 separated in quintiles, Q1 representing genes with the highest RNApII occupancy and Q5 the
1060 lowest. **C.** Metagene analysis of RNApII occupancy over coactivator redundant (CR) genes (top;
1061 n=151) and TFIID-regulated genes (bottom; n=55) longer then 1 kb. Gene classifications are from
1062 Donczew et al. (2020). The Tfb3 configurations are indicated in the key at the bottom: wild-type Tfb3
1063 in red, N-term-Linker + C-term in yellow, N-term + Linker-C-term in blue, and N-term + C-term in
1064 green. To account for the differing lengths of genes, each graph shows 1 kb centered on the
1065 transcription start site (TSS) to the left of the dividing line, and 1 kb centered on the polyadenylation
1066 site (pA) to the right.
1067

Article and Author Information

Author details

Gabriela Giordano
Department of Biological Chemistry and Molecular Pharmacology, Harvard Medical School, Boston, MA, USA
Contribution:; Investigation; Writing – original draft preparation; Visualisation
Competing interests: No competing interests declared.

Robin Buratowski
Department of Biological Chemistry and Molecular Pharmacology, Harvard Medical School, Boston, MA, USA
Contribution: Investigation; Project administration
Competing interests: No competing interests declared.

Célia Jeronimo
Institut de recherches cliniques de Montréal (IRCM), Montréal, Québec, Canada
Contribution: Formal analysis; Data curation; Investigation; Writing – review & editing; Visualisation
Competing interests: No competing interests declared.

Christian Poitras
Institut de recherches cliniques de Montréal (IRCM), Montréal, Québec, Canada
Contribution: Formal analysis
Competing interests: No competing interests declared.

François Robert
Institut de recherches cliniques de Montréal (IRCM), Montréal, Québec, Canada
Département de Médecine, Université de Montréal, Montréal, Québec, Canada
Division of Experimental Medicine, Medicine, McGill University, Montréal, Québec, Canada
Contribution: Conceptualization; Data curation; Formal analysis; Writing – review & editing; Supervision; Funding acquisition
Competing interests: No competing interests declared.

Stephen Buratowski
Department of Biological Chemistry and Molecular Pharmacology, Harvard Medical School, Boston, MA, USA
Contribution: Conceptualization; Investigation; Writing – original draft preparation; Writing – review & editing; Visualisation; Supervision; Project administration; Funding acquisition
Competing interests: No competing interests declared.
For correspondence: steveb@hms.harvard.edu

Funding

National Institutes of Health (R01GM046498)
Stephen Buratowski

National Institutes of Health (R01GM056663)
Stephen Buratowski

Canadian Institutes of Health Research (PJT-162334)

François Robert

The funders had no role in study design, data collection and interpretation, or the decision to submit the work for publication.

ACKNOWLEDGEMENTS

We are grateful to Steve Hahn (FHCRC, Seattle) and John Feaver (Stanford) for providing several Tfb3 strains and plasmids, and to Jason Tanny (McGill Univ., Montreal) for *S. pombe* cells.

Figure 1 - Figure Supplement 1

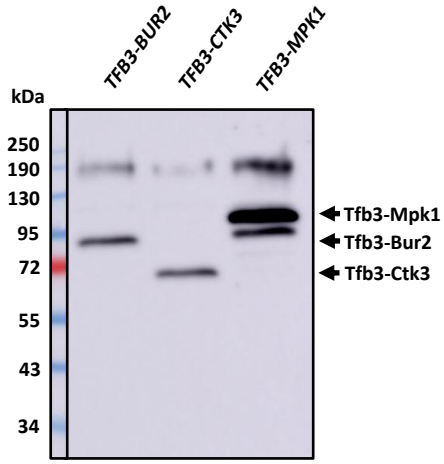

Figure 1

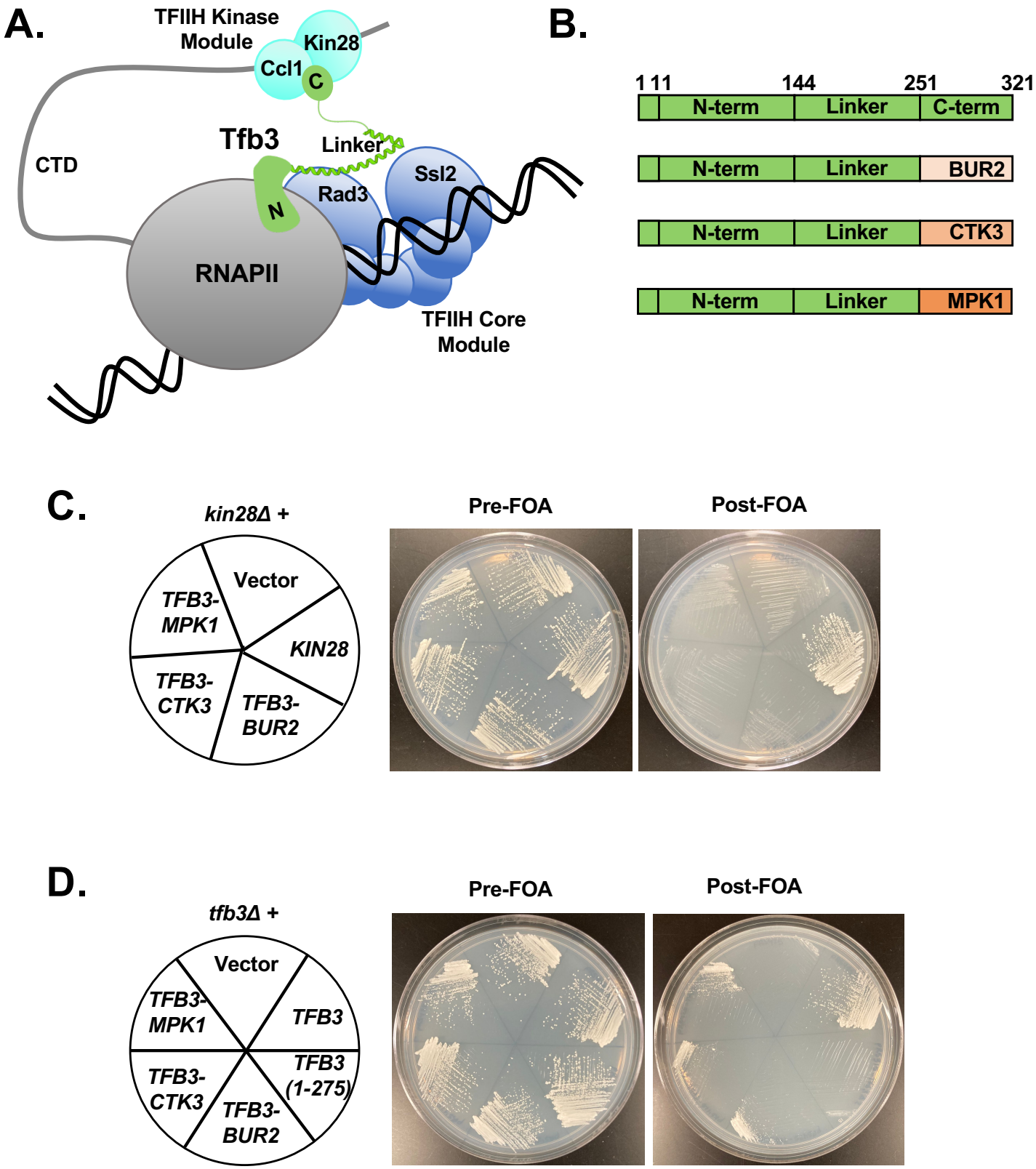
A.
TFIIH Kinase Module
Kin28
Ccl1
C
CTD
Tfb3
Linker
N
Rad3
Ssl2
RNAPII
TFIIH Core Module
B.
1 11
144
251
321
N-term
Linker
C-term
N-term
Linker
BUR2
N-term
Linker
CTK3
N-term
Linker
MPK1
C.
kin28Δ +
Vector
TFB3-MPK1
KIN28
TFB3-CTK3
TFB3-BUR2
Pre-FOA
Post-FOA
D.
tfb3Δ +
Vector
TFB3-MPK1
TFB3
TFB3-CTK3
TFB3-BUR2
TFB3 (1-275)
Pre-FOA
Post-FOA

Figure 2

A.

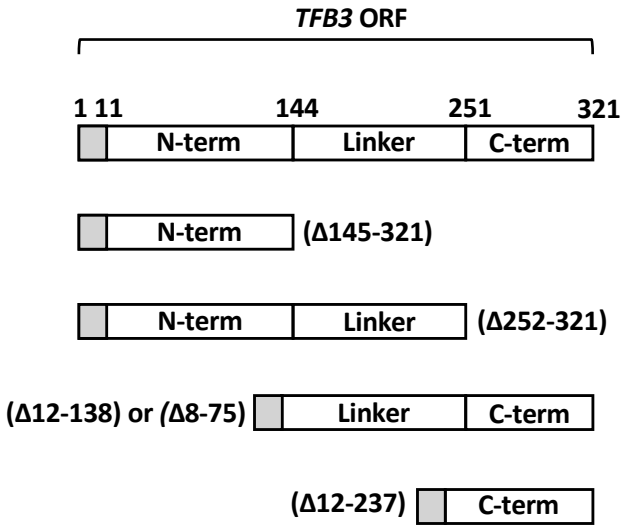
TFB3 ORF
1 11
144
251
321
N-term
Linker
C-term
N-term
(Δ145-321)
N-term
Linker
(Δ252-321)
(Δ12-138) or (Δ8-75)
Linker
C-term
(Δ12-237)
C-term

B.

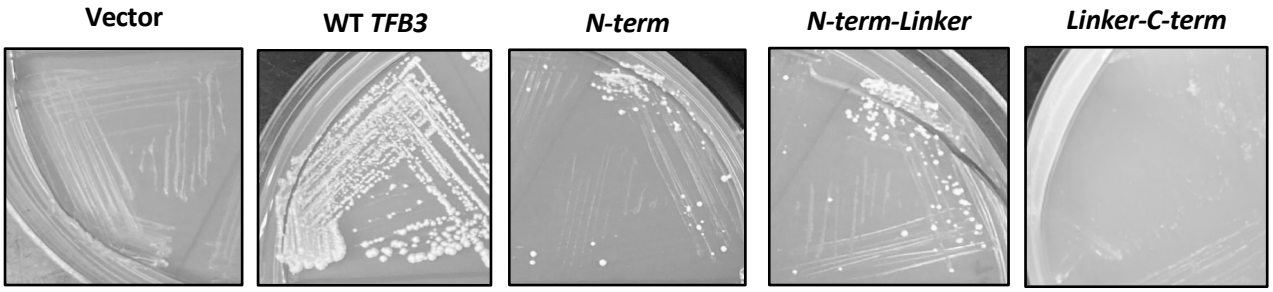
Vector
WT TFB3
N-term
N-term-Linker
Linker-C-term

C.

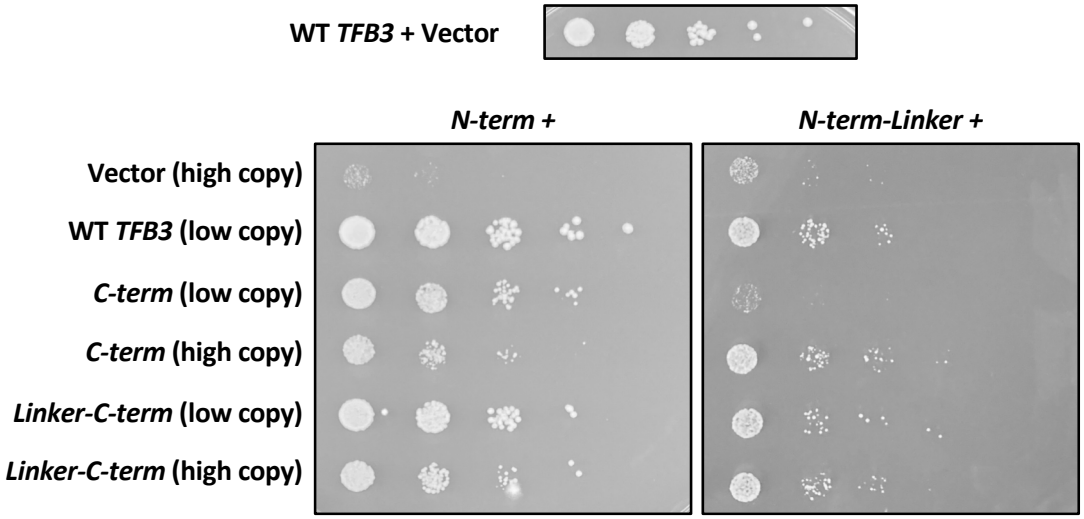
WT TFB3 + Vector
N-term +
N-term-Linker +
Vector (high copy)
WT TFB3 (low copy)
C-term (low copy)
C-term (high copy)
Linker-C-term (low copy)
Linker-C-term (high copy)

Figure 3 - figure supplement 1

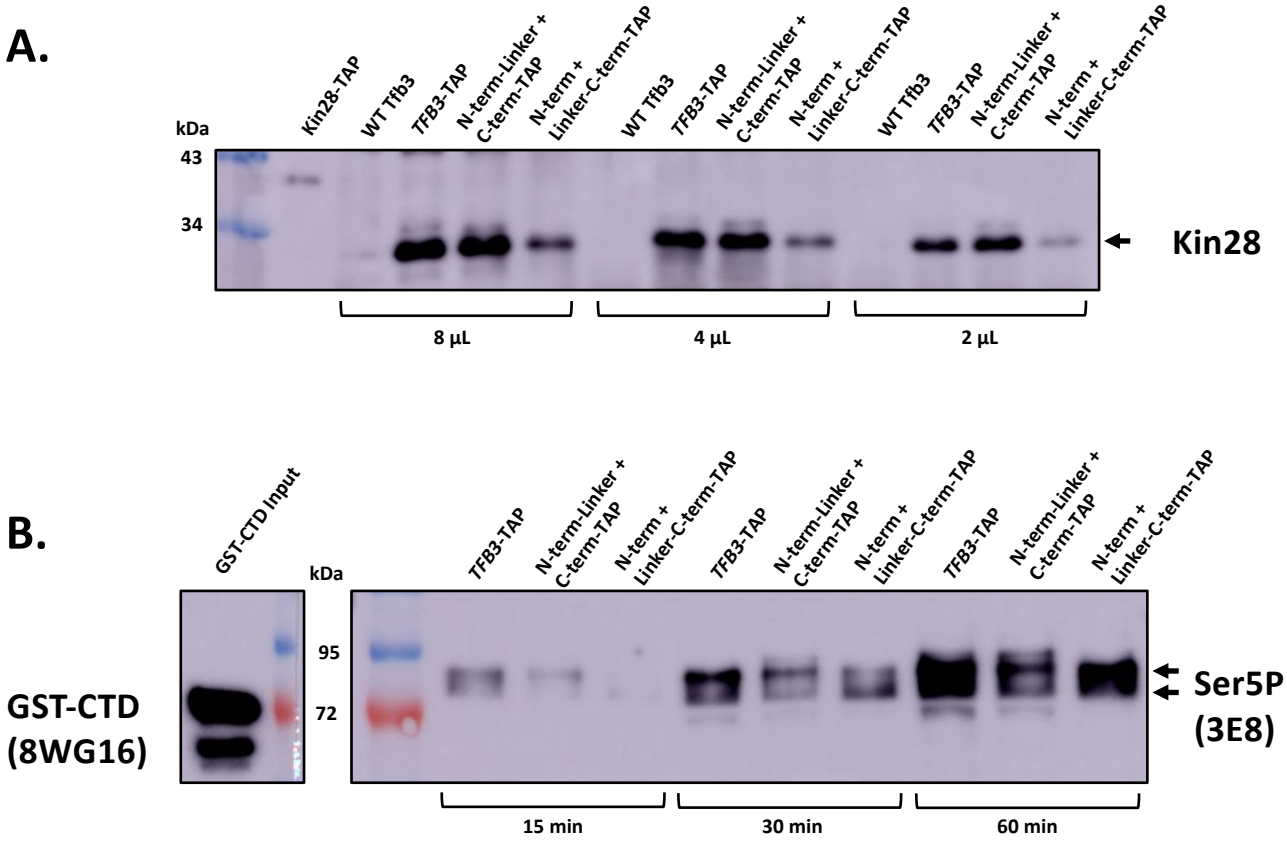

Figure 3

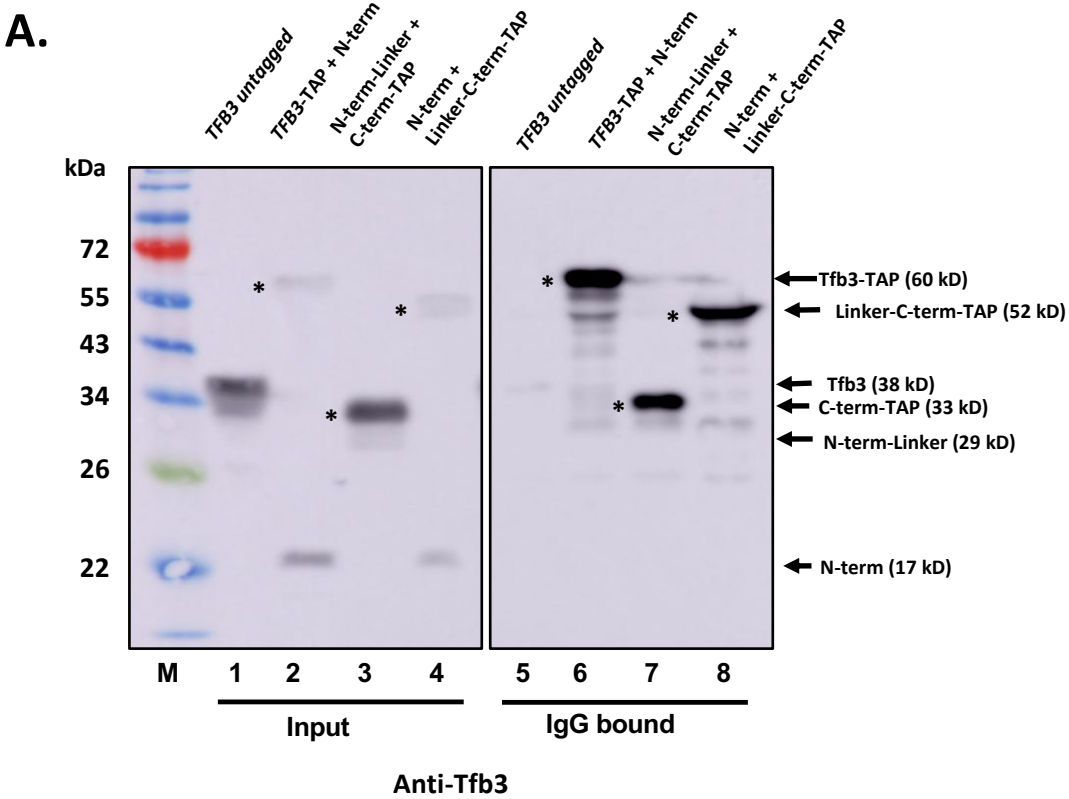
A.
TFB3 untagged
TFB3-TAP + N-term
N-term-Linker + C-term-TAP
N-term + Linker-C-term-TAP
kDa
72
55
43
34
26
22
Tfb3-TAP (60 kD)
Linker-C-term-TAP (52 kD)
Tfb3 (38 kD)
C-term-TAP (33 kD)
N-term-Linker (29 kD)
N-term (17 kD)
M 1 2 3 4 5 6 7 8
Input
IgG bound
Anti-Tfb3

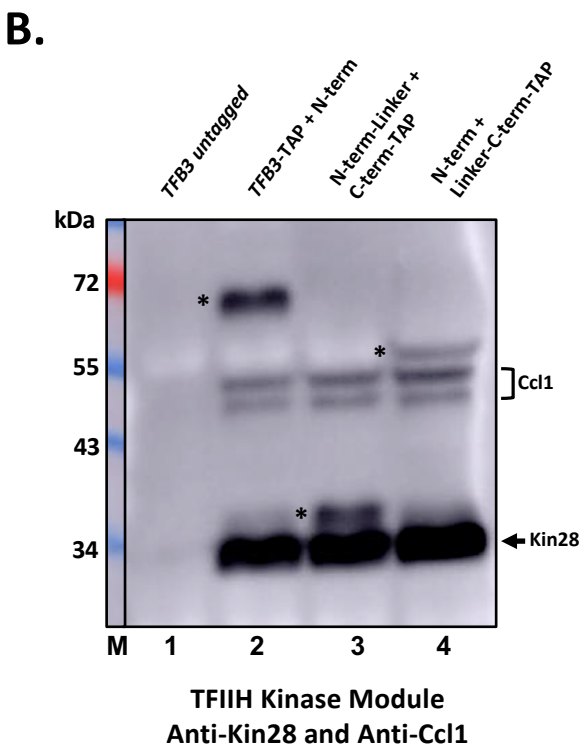
B.
TFB3 untagged
TFB3-TAP + N-term
N-term-Linker + C-term-TAP
N-term + Linker-C-term-TAP
kDa
72
55
43
34
Ccl1
Kin28
M 1 2 3 4
TFIIH Kinase Module
Anti-Kin28 and Anti-Ccl1

Figure 4

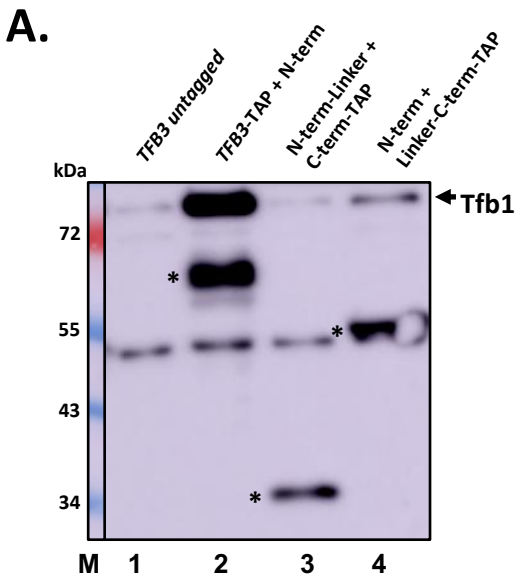

TFIIH Core Module
Anti-Tfb1

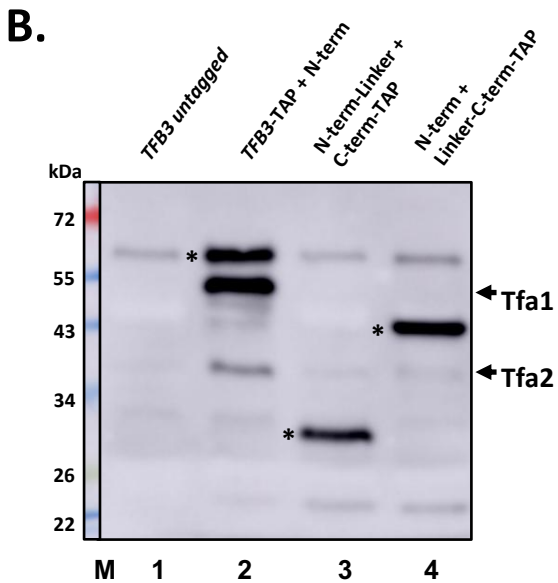

TFIIE
Anti-Tfa1 and Anti-Tfa2

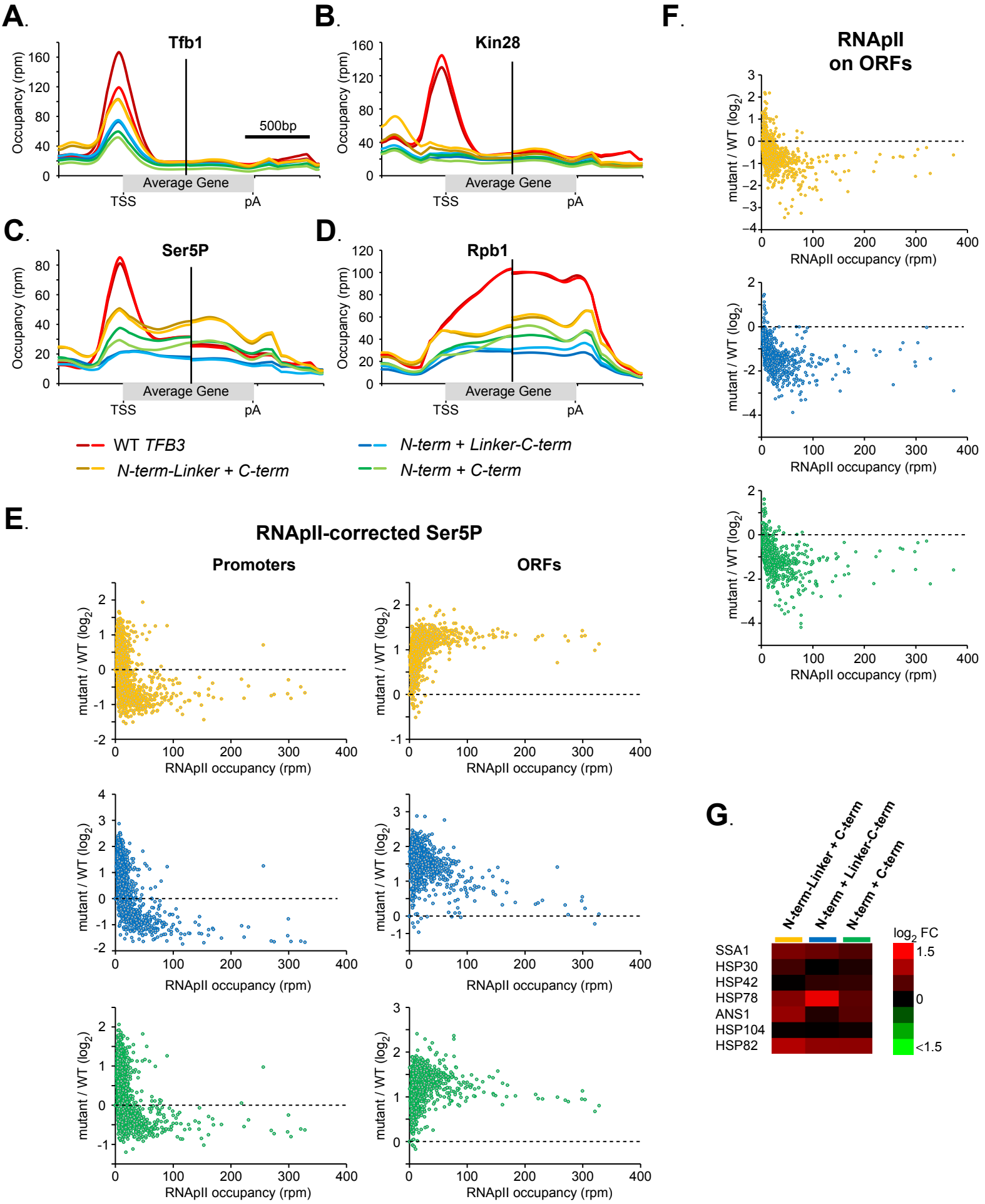

Figure 5 - figure supplement 1

Figure 5 - figure supplement 2

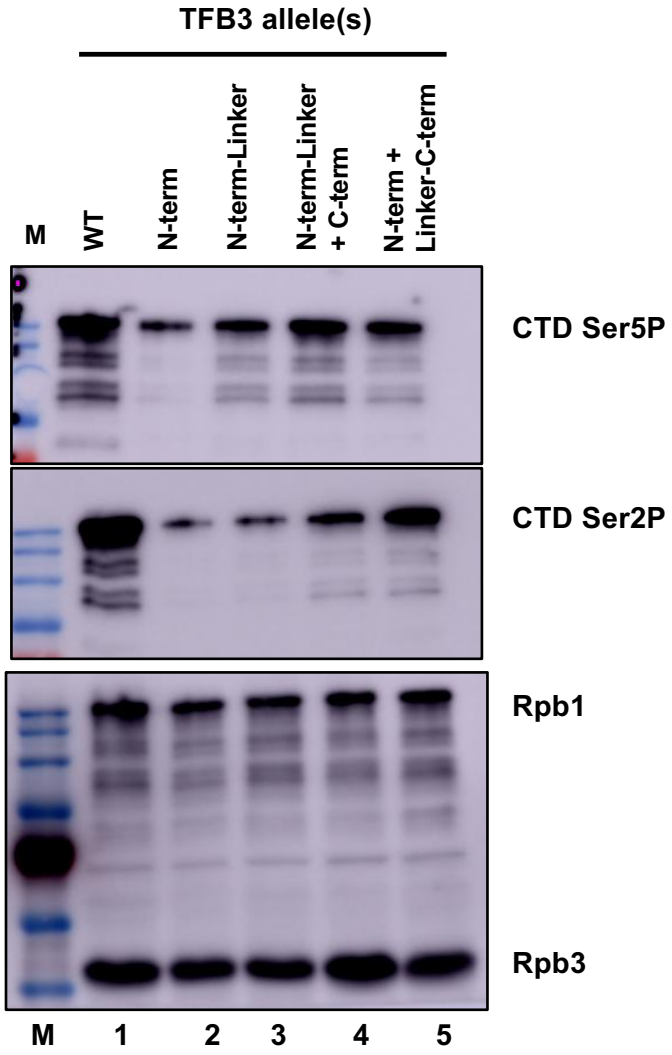

Figure 5 - figure supplement 3

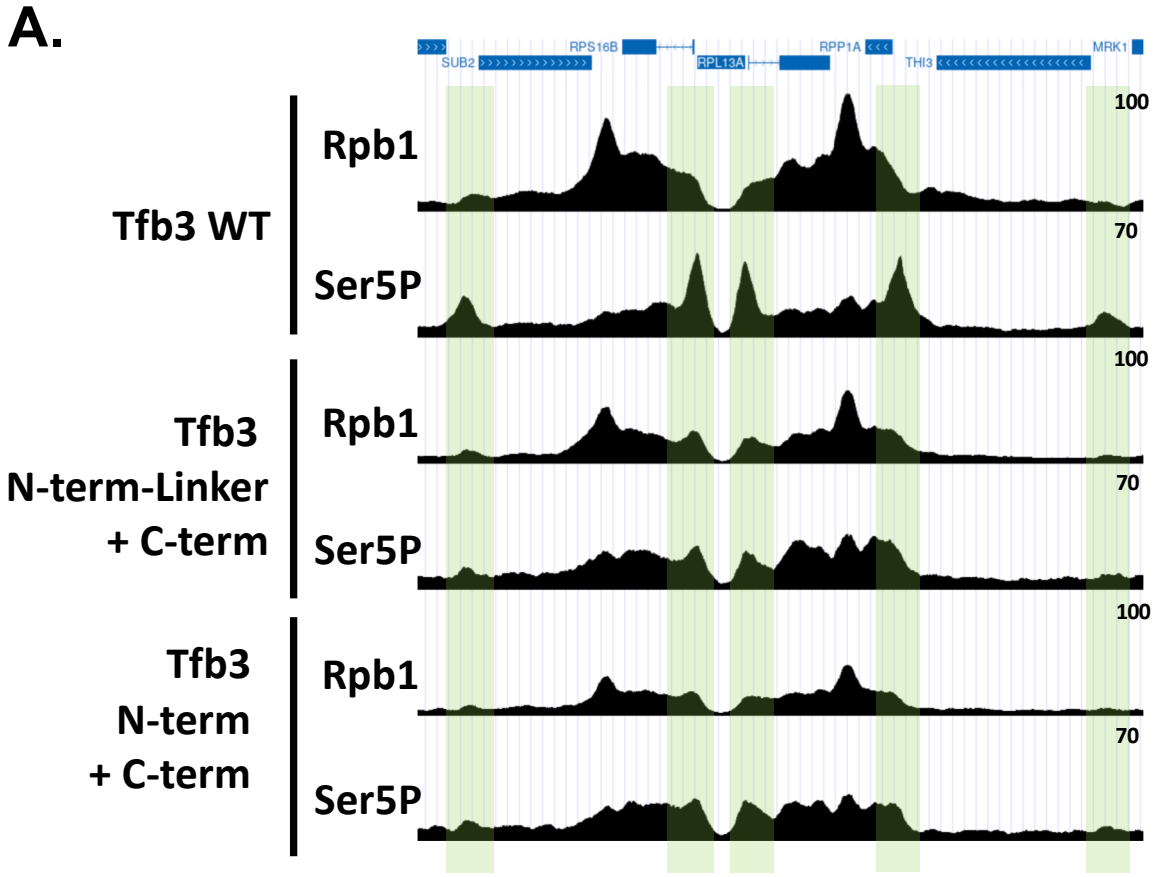

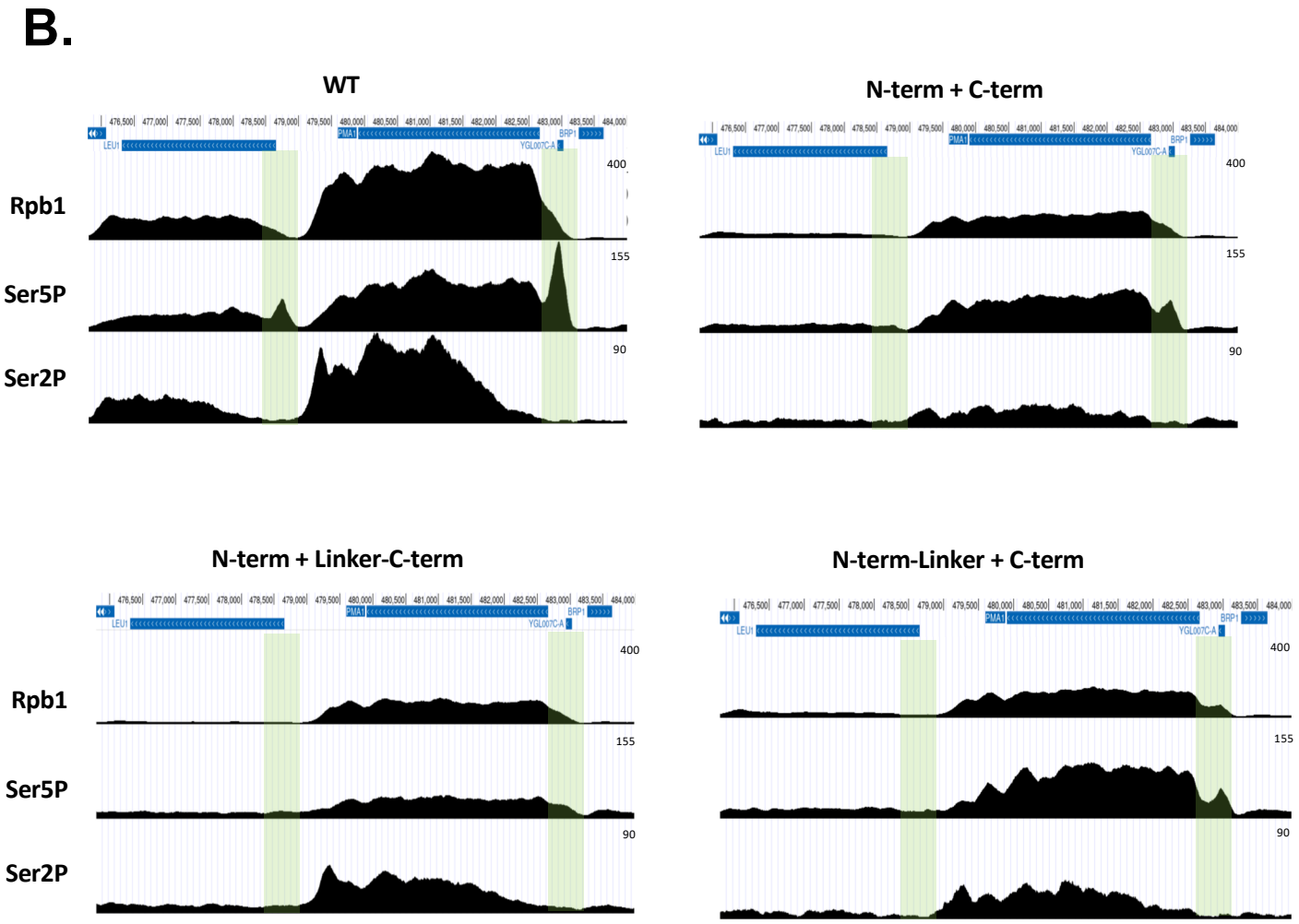

Figure 5 - figure supplement 4

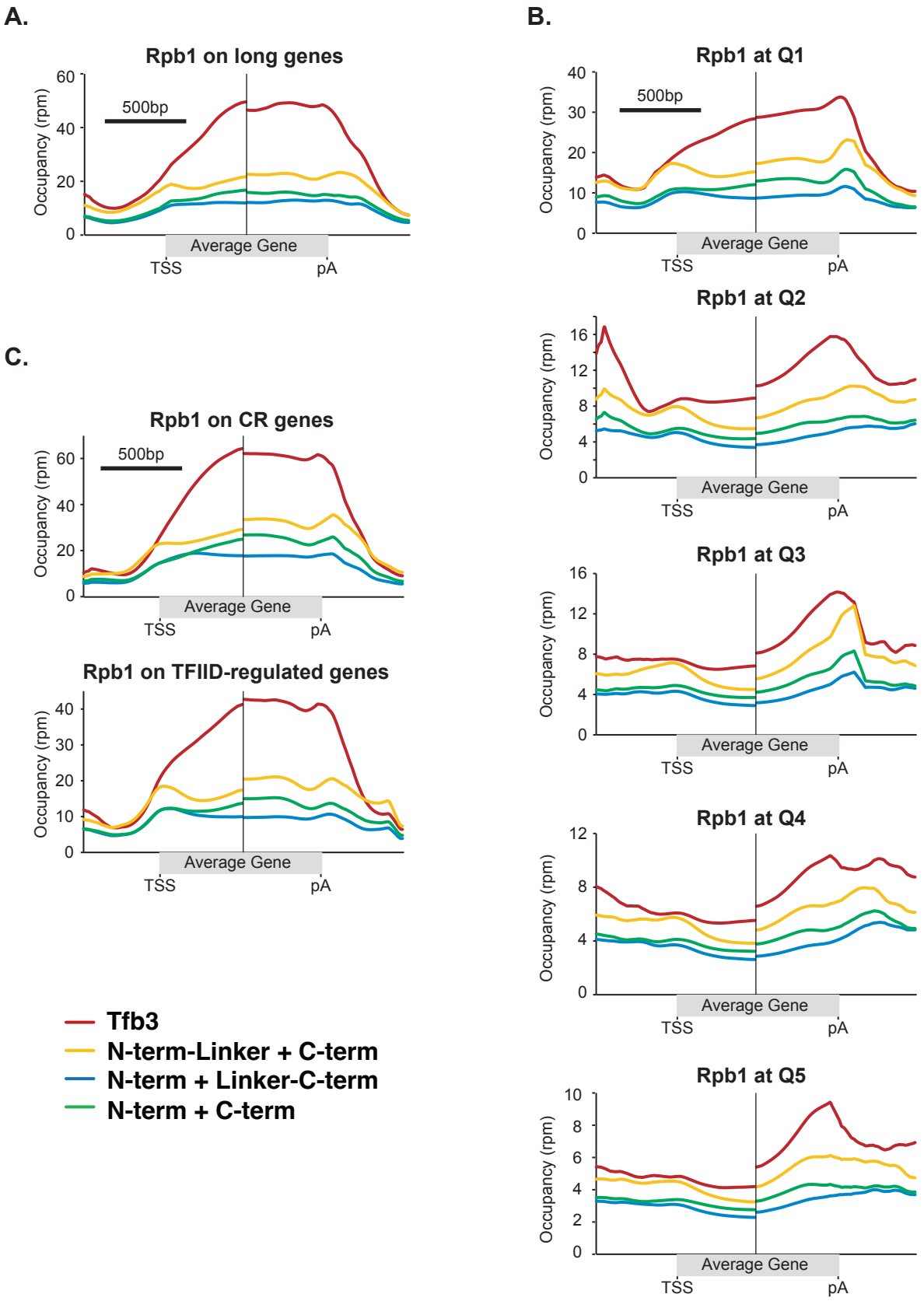

Figure 5

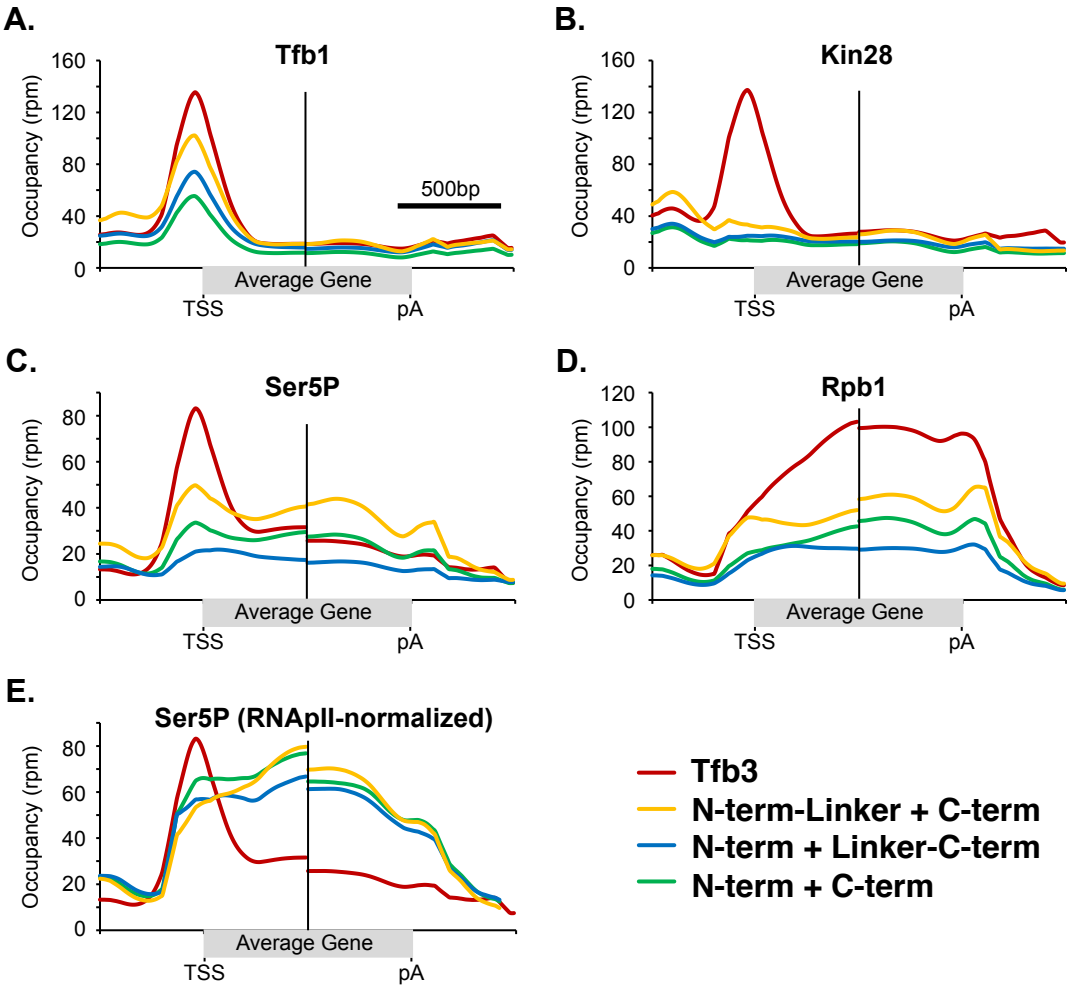
A.
Tfb1
Occupancy (rpm)
160
120
80
40
0
500bp
Average Gene
TSS
pA
B.
Kin28
Occupancy (rpm)
160
120
80
40
0
Average Gene
TSS
pA
C.
Ser5P
Occupancy (rpm)
80
60
40
20
0
Average Gene
TSS
pA
D.
Rpb1
Occupancy (rpm)
120
100
80
60
40
20
0
Average Gene
TSS
pA
E.
Ser5P (RNApII-normalized)
Occupancy (rpm)
80
60
40
20
0
Average Gene
TSS
pA
Tfb3
N-term-Linker + C-term
N-term + Linker-C-term
N-term + C-term

Figure 6

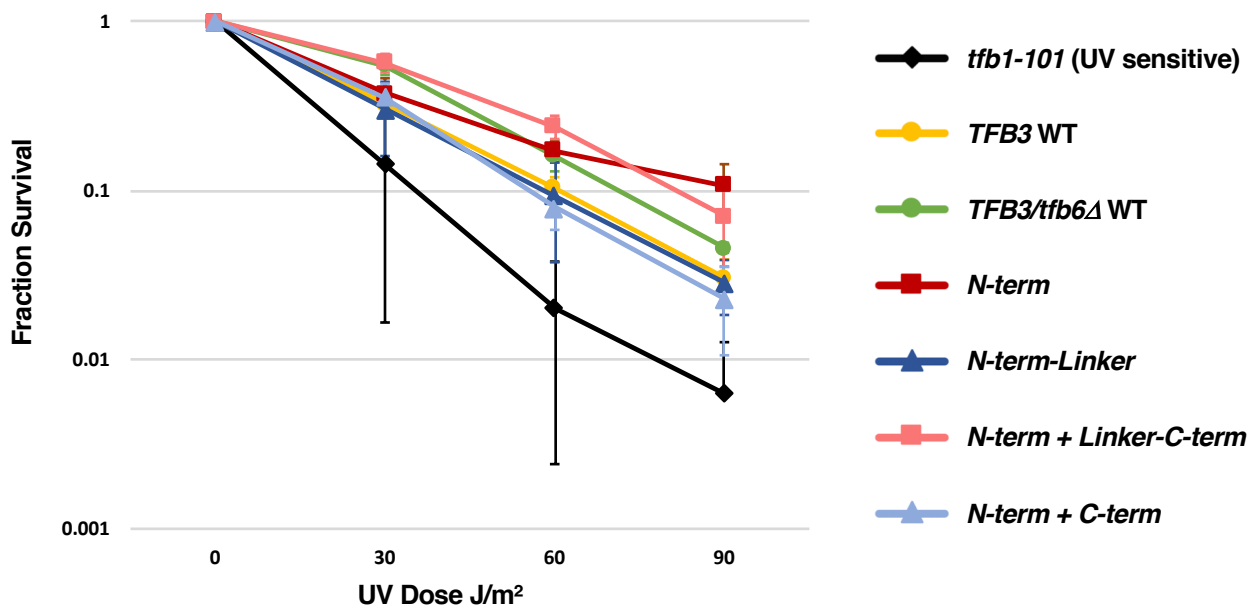
Fraction Survival
1
0.1
0.01
0.001
0
30
60
90
UV Dose J/m²
tfb1-101 (UV sensitive)
TFB3 WT
TFB3/tfb6Δ WT
N-term
N-term-Linker
N-term + Linker-C-term
N-term + C-term

Figure 7

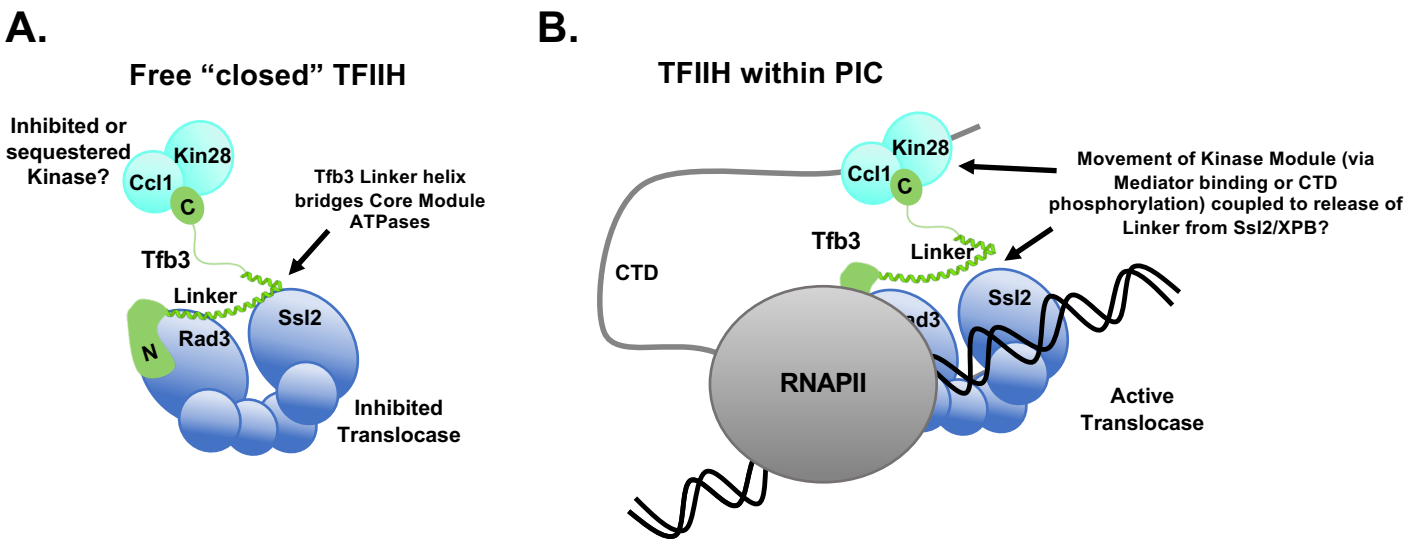
A.
Free "closed" TFIIH
Inhibited or sequestered Kinase?
Kin28
Ccl1
C
Tfb3 Linker helix bridges Core Module ATPases
Tfb3
Linker
Ssl2
Rad3
N
Inhibited Translocase
B.
TFIIH within PIC
Kin28
Ccl1
C
Movement of Kinase Module (via Mediator binding or CTD phosphorylation) coupled to release of Linker from Ssl2/XPB?
CTD
Tfb3
Linker
Ssl2
RNAPII
Active Translocase